

Gravitationally Induced UV Completion of an $O(N)$ Scalar Theory

Alfio M. Bonanno* and Emilio Glaviano†

INAF Osservatorio Astrofisico di Catania,

Via S.Sofia 78, 95123 Catania ITALY

and INFN, Sezione di Catania, Italy

We investigate the ultraviolet completion of an $O(N)$ scalar field theory non-minimally coupled to gravity using the Wilsonian functional renormalization group in the proper-time formulation. Focusing on the spontaneously broken phase, we study the RG flow of the scalar potential and the non-minimal curvature coupling expanded around a running minimum. We identify two distinct classes of fixed-point solutions, one of which is ultraviolet attractive and characterized by a vanishing quartic coupling together with finite, interacting gravitational couplings. For a finite region of infrared initial conditions, the RG trajectories remain regular at all scales and approach this fixed point. This mechanism renders the theory asymptotically safe and leads to a flat scalar potential in the ultraviolet. We show that this mechanism is robust under changes of cutoff scheme and truncation, allowing the ultraviolet completion requirement to constrain the infrared values of the scalar couplings and the mass scale in the broken phase.

* alfio.bonanno@inaf.it

† emilio.glaviano@inaf.it

I INTRODUCTION

Quantum scalar field theories in four dimensions generically face the Landau-pole problem associated with the running of the quartic self-interaction λ . In practice, a Landau pole signals that the low-energy description cannot be extrapolated indefinitely and that new degrees of freedom or a non-perturbative ultraviolet (UV) completion must enter at sufficiently high scales. In the Standard Model the perturbative running of the Higgs quartic coupling is substantially altered by the top-quark Yukawa interaction: the Landau pole is avoided, but λ turns negative around an RG scale of 10^{10} GeV and subsequently evolves only slowly [1]. Nevertheless, additional scalar fields beyond the Higgs are widely expected. They may play a role in inflation [2–8], dark energy [9, 10], or dark matter [11, 12], and in such sectors the Standard-Model Yukawa couplings to fermions may be absent or highly suppressed. It is therefore natural to ask whether *gravity alone*, coupled to scalars, can provide a mechanism that renders the theory UV finite, or whether fermionic interactions are essential as in the Standard Model.

Scalar–tensor theories offer a minimal setting to address this question [13–20]. A particularly interesting case arises when scalars are non-minimally coupled through a term $\xi_{ij}\phi_i\phi_jR$, or more generally via $F(\phi)R$, which ties the running of the non-minimal coupling to the running of the scalar potential in the functional renormalization group (FRG) framework [21–24]. In the symmetry-broken phase, the presence of ξ_{ij} can have important implications at scales above the Planck mass m_p [21–27]. The RG flow of ξ has been studied for $N = 1$ in [25] and for general $F(\phi)R + U(\phi)$ systems in [26] using Wetterich-type flows [28–30]. However, those investigations focused on the infrared (IR) regime, since the gravitational part of the Hessian was neglected and only scalar fluctuations were retained. In contrast, in the UV regime $m_p^2 \ll p^2$ gravitational fluctuations can dominate the dynamics, especially if gravity itself exhibits an interacting fixed point. This possibility underlies the asymptotic-safety scenario for gravity–matter systems [31–33] and, in the context of the Standard Model, motivates the so-called *flatland* scenario in which gravity drives the Higgs quartic coupling to zero at high scales [22, 24, 27, 32, 34–36], building on earlier ideas [37, 38]; see [39, 40] for recent reviews. Related evidence that quantum gravity can cure Landau-pole behavior have been found, for instance, in studies of the Abelian gauge sector [41–43].

An interacting UV completion can also make low-energy physics predictive. In the Standard-Model context, the approach to a gravity-induced UV fixed point can correlate IR values of couplings and masses, with early examples including bounds on the Higgs mass [27] and quark-

mass relations [32, 36], as well as predictions for Abelian gauge couplings [42–44]. Beyond the Higgs sector, asymptotic safety may also shed light on dark-matter model building [45–48], where a scalar dark sector could be driven to an interacting UV regime by gravitational fluctuations.

In this paper, we study an $O(N)$ scalar theory non-minimally coupled to gravity of the form $F(\phi)R + U(\phi)$ and investigate whether gravity alone can render the theory UV finite. We work in a Wilsonian setting using the proper-time (PT) formulation of the functional RG [49–63]. The PT flow for the Wilsonian action S_Λ reads

$$\Lambda \partial_\Lambda S_\Lambda[\phi] = \frac{1}{2} \int_0^\infty \frac{ds}{s} r(s, \Lambda^2 Z_\Lambda) \text{Tr} \left[e^{-sS_\Lambda^{(2)}} \right], \quad (\text{I.1})$$

where Λ is the Wilsonian UV cutoff, $S_\Lambda^{(2)}$ the Hessian, Z_Λ the wave-function renormalizations, and r a cutoff kernel. We employ the spectrally adjusted cutoff family discussed in [64],

$$r(s, \Lambda^2 Z_\Lambda) = \left(2 + \epsilon \frac{\Lambda \partial_\Lambda Z_\Lambda}{Z_\Lambda} \right) \frac{(s \gamma \Lambda^2 Z_\Lambda)^m}{\Gamma(m)} e^{-s \gamma \Lambda^2 Z_\Lambda}, \quad (\text{I.2})$$

where $m > 0$ controls the shape in the interpolation region, $\gamma \in \{m, 1\}$ labels two cutoff families, and $\epsilon \in \{0, 1\}$ distinguishes type-C ($\epsilon = 0$) from type-B ($\epsilon = 1$) cutoffs; throughout this work we adopt the type-C choice, which is known to yield highly accurate critical exponents at the Wilson-Fisher fixed point [52, 58] but also in the pure gravitational sector [65].

Our goal is to determine under which conditions the coupled scalar–gravity system becomes asymptotically safe, thereby providing a concrete realization of a gravity-induced mechanism that renders the scalar sector UV complete. We analyze the fixed-point structure, the critical properties, and the global behavior of RG trajectories in the symmetry-broken phase, identifying a finite region of infrared initial data that flows to a UV-attractive fixed point with vanishing quartic coupling.

The paper is organized as follows. In Sec. II we introduce the model and the approximation scheme. In Sec. III we present the beta functions and discuss their structure. In Sec. IV we analyze the fixed points and critical exponents. In Sec. V we explain the basic physical mechanism and delineate the UV-complete region of initial conditions. In Sec. VI we present numerical solutions and discuss the resulting predictions. We summarize our conclusions in Sec. VII. Appendix A provides the derivation of the flow equations for the wave-function renormalizations, while Appendix B collects the explicit beta functions used throughout the paper.

II FORMALISM

A The theory

We consider an $O(N)$ -invariant scalar multiplet $\Phi_a = (\phi_1, \dots, \phi_N)$ non-minimally coupled to gravity through a Wilsonian action of the form

$$S_\Lambda[g, \Phi] = \int d^d x \sqrt{g} \left(-F_\Lambda(\rho) R + \frac{1}{2} Z_T(\Lambda) \sum_{a=1}^{N-1} \phi_a (-\square) \phi_a + \frac{1}{2} Z_L(\Lambda) \phi_N (-\square) \phi_N + U_\Lambda(\rho) \right), \quad (\text{II.1})$$

where $-\square$ is the Laplace–Beltrami operator acting on the scalar fields and ρ denotes the invariant

$$\rho = \frac{1}{2} \Phi_a \Phi_a = \frac{1}{2} \sum_{a=1}^N \phi_a^2. \quad (\text{II.2})$$

We work in the broken phase and choose the background direction to lie along the N -th component. Accordingly, we decompose the multiplet into one longitudinal (radial) field and $N-1$ transverse (Goldstone) fields,

$$\Phi_a = \phi_N n_a + \pi_a, \quad n_a = \delta_{aN}, \quad n \cdot \pi = 0. \quad (\text{II.3})$$

Equivalently, introducing the longitudinal and transverse projectors (defined with respect to the chosen direction n_a),

$$P_{ab}^L = n_a n_b, \quad P_{ab}^T = \delta_{ab} - n_a n_b, \quad (\text{II.4})$$

one has $\phi_N = P_{Nb}^L \Phi_b$ and $\pi_a = P_{ab}^T \Phi_b$ (with $a = 1, \dots, N-1$).

In eq. (II.1) we allow for two (scale-dependent but field-independent) wave-function renormalizations, $Z_L(\Lambda)$ for the longitudinal mode and $Z_T(\Lambda)$ for the transverse modes. This corresponds to the LPA'-type approximation for the scalar sector. The associated anomalous dimensions are

$$\eta_T(\Lambda) = -\frac{\Lambda \partial_\Lambda Z_T(\Lambda)}{Z_T(\Lambda)}, \quad \eta_L(\Lambda) = -\frac{\Lambda \partial_\Lambda Z_L(\Lambda)}{Z_L(\Lambda)}, \quad (\text{II.5})$$

so that the (RG) scaling dimensions of transverse and longitudinal fields differ,

$$[\phi_a] = \frac{d-2+\eta_T}{2}, \quad [\phi_N] = \frac{d-2+\eta_L}{2}. \quad (\text{II.6})$$

B The proper-time flow equations

The proper-time flow equations for F and U at $Z = 1$ have been derived in [66] using the background-field method and the heat-kernel expansion, with linear splitting for the scalar and exponential splitting for the metric, in the physical gauge [67, 68]. The flow equations for Z_L and Z_T follow from the same setup; details are given in Appendix A. It is convenient to introduce the ratio

$$w(\Lambda) = \frac{Z_T(\Lambda)}{Z_L(\Lambda)}, \quad (\text{II.7})$$

which measures the relative normalization of transverse and longitudinal modes. Its RG evolution is governed by

$$\Lambda \partial_\Lambda w = w(\eta_L - \eta_T). \quad (\text{II.8})$$

or equivalently by $\Lambda \partial_\Lambda \ln w = \eta_L - \eta_T$.

Introducing the dimensionless variables

$$x = Z_L \Lambda^{2-d} \rho, \quad u_\Lambda(x) = \Lambda^{-d} U_\Lambda(\rho), \quad f_\Lambda(x) = \Lambda^{2-d} F_\Lambda(\rho), \quad (\text{II.9})$$

we obtain the dimensionless flow equations for u_Λ and f_Λ ,

$$\begin{aligned} \dot{u} &= -d u + (d - 2 + \eta_L) x u' + \alpha \left(2d(d - 3) + 4(N - 1) \left(1 + \frac{u'}{\gamma w} \right)^{\frac{d}{2}-m} + 4 \mathcal{P}^{\frac{d}{2}-m} \right), \\ \dot{f} &= (2 - d) f + (d - 2 + \eta_L) x f' - \frac{\alpha(d - 2m)}{12\gamma} \left(72 + 6d - 2d^2 - \right. \\ &\quad \left. - 4(N - 1) \left(1 + \frac{6f'}{w} \right) \left(1 + \frac{u'}{\gamma w} \right)^{\frac{d}{2}-m-1} - 4 \mathcal{Q} \mathcal{P}^{\frac{d}{2}-m-1} \right), \end{aligned} \quad (\text{II.10})$$

where

$$\begin{aligned} \alpha &= \frac{\gamma^{d/2} \Gamma(m - \frac{d}{2})}{4(4\pi)^{d/2} \Gamma(m)}, \\ \mathcal{P} &= 1 + \frac{u' + 2xu''}{\gamma \left(1 + \frac{4(d-1)x(f')^2}{(d-2)f} \right)}, \quad \mathcal{Q} = 1 + \frac{6 \left(f' + \frac{4x(f')^2}{(d-2)f} + 2xf'' \right)}{1 + \frac{4(d-1)x(f')^2}{(d-2)f}}. \end{aligned} \quad (\text{II.11})$$

Here a prime denotes a derivative with respect to x , and a dot denotes a derivative with respect

to RG time $t = \ln(\Lambda/\Lambda_0)$, with Λ_0 an arbitrary reference scale.

The anomalous dimensions read

$$\begin{aligned} \eta_L &= \frac{\gamma^{\frac{d}{2}-3}}{3(4\pi)^{d/2}} \frac{\Gamma(m - \frac{d}{2} + 3)}{\Gamma(m)} \left(1 + \frac{\bar{u}' + 2\bar{x}\bar{u}''}{\gamma \left(1 + \frac{4(d-1)\bar{x}(\bar{f}')^2}{(d-2)\bar{f}} \right)} \right)^{\frac{d}{2}-(m+3)} \left[\frac{\bar{x}(\bar{u}'')^2}{w^2} (N-1) \right. \\ &\quad \left. + \frac{4\bar{x}^2\bar{u}''' - 3\bar{u}'}{4\bar{x} \left(1 + \frac{4(d-1)\bar{x}(\bar{f}')^2}{(d-2)\bar{f}} \right)^2} \left(1 + \frac{\bar{u}' + 2\bar{x}\bar{u}''}{4\bar{x}^2\bar{u}''' - 3\bar{u}'} \left(1 + \frac{2 \left(1 + \frac{4(d-1)\bar{x}^2\bar{f}'}{(d-2)\bar{f}} \left(\frac{(\bar{f}')^2}{\bar{f}} - 2\bar{f}'' \right) \right)}{1 + \frac{4(d-1)\bar{x}(\bar{f}')^2}{(d-2)\bar{f}}} \right) \right)^2 \right], \\ \eta_T &= \frac{\gamma^{\frac{d}{2}-3}}{6(4\pi)^{d/2} \bar{x} w} \frac{\Gamma(m - \frac{d}{2} + 3)}{\Gamma(m)} \left(1 + \frac{\bar{u}'}{\gamma w} \right)^{\frac{d}{2}-(m+3)} \left(\frac{\bar{u}'}{w} - \frac{\bar{u}' + 2\bar{x}\bar{u}''}{1 + \frac{4(d-1)\bar{x}(\bar{f}')^2}{(d-2)\bar{f}}} \right)^2. \end{aligned} \tag{II.12}$$

A bar indicates that the corresponding quantity is evaluated on the background configuration used in the derivation of the flow (see Appendix A).

III THE PROPERTIES OF THE RG FLOW

A The truncation

Building on the fixed-point analysis of Eq. (II.10) at $Z = 1$, it was shown in [66] that $u_* = u_0$ and $f_*(x) = f_0 + f_1 x$ provide an exact scaling solution, both for $f_0 \neq 0$ and for $f_0 = 0$. Away from the fixed point these functions acquire a non-trivial RG-time dependence: the running of f can be parametrized by $f_0(t)$ and $f_1(t)$, while the potential develops a non-trivial x -dependence that we encode in a polynomial expansion. We focus on the spontaneously broken phase and write

$$u_t(x) = u_0(t) + \lambda(t)(x - x_0(t))^2 \tag{III.1}$$

where $x_0(t)$ denotes the running vacuum expectation value (vev), defined by $u'_t(x_0) = 0$. With this convention one has

$$u''_t(x_0) = 2\lambda(t). \tag{III.2}$$

Without loss of generality we choose the vev to point in the N direction, so that only the longitudinal scalar mode acquires an expectation value. Accordingly, we parametrize the $O(N)$

multiplet as

$$\Phi_i = (v + \sigma) n_i + \pi_i, \quad i = 1, \dots, N, \quad n_i = \delta_{iN}, \quad n \cdot \pi = 0, \quad (\text{III.3})$$

and the relation between v and x_0 reads $x_0 = Z_L \Lambda^{2-d} v^2 / 2$.

The physical mass of the longitudinal fluctuation in the broken phase is, for general u and f ,

$$m_\sigma^2 = \Lambda^2 \frac{2x_0 u_t''(x_0)}{1 + \frac{4(d-1)x_0 [f_t'(x_0)]^2}{(d-2) f_t(x_0)}}. \quad (\text{III.4})$$

The $N - 1$ transverse fields become Goldstone bosons and remain massless. Since $m_\sigma^2 > 0$ and we require $u_t''(x_0) > 0$ for a positive-definite Hamiltonian, Eq. (III.4) implies that $x_0 > 0$.

For $f_t(x) = f_0(t) + f_1(t)x$ the dimensionless Planck mass is

$$\tilde{m}_p^2(t) = f_t(x_0) = f_0(t) + f_1(t)x_0, \quad (\text{III.5})$$

and we can write

$$f_t(x) = \tilde{m}_p^2(t) + f_1(t)(x - x_0(t)). \quad (\text{III.6})$$

In the absence of f_1 the inverse of \tilde{m}_p^2 corresponds to the dimensionless Newton coupling. We therefore set $\tilde{m}_p^2(t) = 1/g(t)$. With these substitutions, the dimensionless mass corresponding to Eq. (III.4) becomes

$$\tilde{m}_\sigma^2 = \frac{4x_0 \lambda}{1 + \frac{4(d-1)x_0 f_1^2}{(d-2) \tilde{m}_p^2}} = \frac{4x_0 \lambda}{1 + \frac{4(d-1)g x_0 f_1^2}{d-2}}. \quad (\text{III.7})$$

In the absence of gravitational interactions, or for $f_1 = 0$, this reduces to the standard result.

B The conditions on the flow of λ for a regular running

The beta functions for u_0 , x_0 , λ , g , f_1 , and w are derived in Appendix B. For the present discussion we focus on the flow of λ . Generally, the flow is composed by two contributions:

$$\dot{\lambda}(t) = \beta_g(t) + \beta_m(t), \quad (\text{III.8})$$

where β_g and β_m are the gravitational and matter contribution to the flow respectively. In particular, the two contributions can be written as

$$\beta_g(t) = -A(t)\lambda(t), \quad \beta_m(t) = \eta_L(t)\lambda(t) + b(t)\lambda^2(t) \quad (\text{III.9})$$

where in $d = 4$ the two coefficients A and b are given by

$$A(t) = -\frac{9\gamma f_1^2 g (1 - f_1 g x_0) (1 + 2f_1 g x_0 (f_1 - \frac{1}{3}))}{4\pi^2(m-1) (1 + 6f_1^2 g x_0)^3 \left(1 + \frac{4\lambda x_0}{\gamma(1+6f_1^2 g x_0)}\right)^m},$$

$$b(t) = \frac{1}{8\pi^2(m-1)} \left(\frac{(m-1)(N-1)}{w^2} + \frac{3C(t)}{(1 + 6f_1^2 g x_0)^4 \left(1 + \frac{4\lambda x_0}{\gamma(1+6f_1^2 g x_0)}\right)^m} \right), \quad (\text{III.10})$$

$$C(t) = 3(m-1) + 12g(1+m)f_1^2 x_0 + 4f_1^3 g^2 x_0^2 (6m-16 + 3(3+m)f_1) + 16f_1^4 g^3 x_0^3 (1+3(m-2)f_1) + 48f_1^6 g^4 x_0^4 (m-1).$$

The expression for $\eta_L(t)$ is given in Eq. (B.9). This contributes with a term $\eta_L \sim \lambda^2$ so the piece $\lambda\eta_L$ is actually of the third order in λ . It is convenient to write the matter contribution as

$$\beta_m(t) = \eta_L(t)\lambda(t) + b(t)\lambda^2(t) = (D(t)\lambda(t) + b(t))\lambda^2(t) \equiv B(t)\lambda^2(t) \quad (\text{III.11})$$

where we used $\eta_L(t) = D(t)\lambda^2(t)$. The expression for $D(t)$ can be read from eq. (B.9).

The presence of a non-vanishing non-minimal parameter f_1 couples λ to the gravitational sector through the linear term proportional to $A(t)$. For $f_1 = 0$ one recovers the purely scalar structure, in which gravity does not affect the familiar one-loop form and the coefficient $b(t)$ of λ^2 in $\beta_m(t)$ is positive. In the present truncation and for the parameter range considered in this work, the coefficient $b(t)$ remains positive for $f_1 \neq 0$ too. Furthermore, it turns out that $D(t) \geq 0$ always and accordingly $B(t) > 0$, therefore the matter contribution to the flow of λ always drives the solution to a singularity in this case.

The linear term in β_g can be interpreted as providing an effective scaling contribution for λ . With the convention in Eq. (III.8), antiscreening corresponds to $A(t) > 0$, since then the term $\beta_g(t) = -A(t)\lambda$ drives λ towards smaller values as the RG scale increases. Since $x_0 > 0$ and $g > 0$, the gravitational contribution to $A(t)$ can change sign only for $f_1 > 0$. If $A(t)$ becomes positive and dominates the dynamics from some scale \bar{t} up to $t \rightarrow \infty$, the singularity is avoided

and λ decreases towards the ultraviolet.

More generally, in many gravity–matter systems gravitational fluctuations can induce anti-screening contributions that weaken matter self-interactions at high scales [22, 24, 27, 31–36]. However, not all RG trajectories are expected to approach a UV fixed point. In our case the relevant question is under which conditions the gravitational fluctuations controlled by f_1 and g overcome the matter fluctuations. From Eq. (III.8) this requires that the linear term becomes sufficiently important compared to the quadratic and cubic term in $B(t)$, so that the flow can enter a regime where λ is driven away from the singularity and towards a scale-invariant trajectory. In such a regime one expects λ to approach an interacting scaling value $\lambda_* = A_*/B_*$ (when $A_* > 0$), after which the inequality $|A| > B\lambda$ ensures a further decrease of λ towards the UV¹.

Since in the low-energy regime one typically has $A < 0$, this mechanism requires a crossover at which the linear term changes sign. Motivated by the explicit factor $(1 - f_1 g x_0)$ appearing in $A(t)$, one may estimate the corresponding condition as

$$f_1^{\text{crit}}(t) = \frac{1}{g(t) x_0(t)}. \quad (\text{III.12})$$

For $f_1(t) \geq f_1^{\text{crit}}(t)$ the linear term can become negative so that $|\beta_g(t)| > \beta_m(t)$, allowing for a positive scaling value $\lambda_* > 0$ and, for sufficiently large t , a decay of λ towards the ultraviolet. Given a numerical solution, Eq. (III.12) also provides an estimate for the scale \bar{t} at which the crossover occurs. The condition $f_1(t) \geq f_1^{\text{crit}}(t)$ together with $|A| > B\lambda$ for $t > \bar{t}$ implies that, instead of growing logarithmically towards the UV, λ decreases according to some inverse power law in t and becomes asymptotically free as $t \rightarrow \infty$.

IV FIXED-POINT AND PERTURBATIONS

A Fixed points

If the conditions discussed in Sec. III are satisfied, λ does not run into a singularity. In fact, the absence of singularities at large RG time requires that the flow approaches a fixed-point regime as $t \rightarrow \infty$. The fixed points therefore provide the main tool to understand the global RG dynamics.

¹ Since both B_* and A_* contain λ , the relation $\lambda_* = B_*/A_*$ has to be interpreted as an equation determining λ_* rather than an explicit determined value of λ_* . Similarly, the inequality $|A| > B\lambda$ has to be interpreted as a condition determining when in the flow of λ the gravitational contribution $\beta_g(t) = -A(t)\lambda(t)$ starts to dominate over the matter contribution $\beta_m(t) = B(t)\lambda^2(t)$, namely when the condition $|\beta_g(t)| > \beta_m(t)$ is reached.

Using the beta functions reported in Appendix B, we find that all fixed points share

$$u_{0*} = \gamma^2 \frac{2+N}{64\pi^2} \frac{\Gamma(m-2)}{\Gamma(m)}, \quad \lambda_* = 0, \quad w_* = a, \quad (\text{IV.1})$$

where w_* is a free parameter, denoted by a . This reflects the fact that at these fixed points one has $\eta_{L*} = 0$ and $\eta_{T*} = 0$, so the ratio $w = Z_T/Z_L$ is not fixed by the flow.

Concerning the remaining couplings x_{0*} , g_* and f_{1*} , we find five fixed points which can be organized into two classes. The first class contains the Gaussian fixed point,

$$x_{0*} = \gamma \frac{N-1+3a}{32\pi^2(m-1)a}, \quad g_* = 0, \quad f_{1*} = b, \quad (\text{IV.2})$$

where also f_{1*} is free (we denote it by b), as well as two interacting, Reuter-type fixed points in the presence of matter,

$$x_{0*} = \gamma \frac{N-1+3a}{32\pi^2(m-1)a}, \quad g_* = \frac{192\pi^2(m-1)}{(16-N)\gamma}, \quad f_{1*} = 0, \quad (\text{IV.3})$$

and

$$x_{0*} = h(N, a, m), \quad g_* = l(N, a, m), \quad f_{1*} = \frac{1}{3}. \quad (\text{IV.4})$$

The second and third fixed points correspond to the values of the exact scaling solutions $u = u_*$ and $f_* = f_0 + f_1 x$ found in [66] for $f_1 = 0$ and $f_1 \neq 0$, respectively, now extended to $Z \neq 1$. For the fixed point with $f_{1*} = 1/3$, the expressions for x_{0*} and g_* are non-trivial functions of N , a and m ; we show them in Figs. 1(a) and 1(b) for $m = 3$ and $\gamma = 1$ as functions of $w_* = a$ for representative values of N .

The second class consists of two fixed points,

$$\begin{aligned} x_{0*} &= \frac{\gamma}{64\pi^2(m-1)} \left(N - 13 + \frac{N-1}{a} \pm \sqrt{A} \right), & g_* &= \frac{192\pi^2(m-1)}{(16-N)\gamma}, \\ f_{1*} &= -\frac{1}{12} \left(1 + \frac{N-13 \pm \sqrt{A}}{N-1} a \right), \end{aligned} \quad (\text{IV.5})$$

where

$$A = (N-13)^2 - \frac{2}{a}(N-19)(N-1) + \frac{1}{a^2}(N-1)^2 \quad (\text{IV.6})$$

These fixed points generalize the exact scaling solutions $u = u_*$ and $f = f_{1*}x$ of [66]. As in [66], the branch with the minus sign for $N < 16$ yields $x_{0*} < 0$ but also $f_{1*} < 0$ throughout the parameter region (see Figs. 2(a) and 2(b)). By contrast, the branch with the plus sign yields $x_{0*} > 0$ and $f_{1*} > 0$ (see Figs. 3(a) and 3(b)). Additionally, only the minus-sign branch admits a regular $N \rightarrow 1$ limit.

A part from the case of the fixed point where $f_{1*} = 1/3$, the fixed point value of g_* is the same in all cases and is given by $g_* = 192\pi^2(m-1)/(\gamma(16-N))$. It is therefore defined only for $N \neq 16$ and becomes negative for $N > 16$. Furthermore, as for the scaling solutions in [66], for all fixed points the value of f_{1*} does not depend on m and, accordingly, not on γ .

The family structure of the fixed point does not depend on γ . The fact that qualitative fixed-point physics does not depend on γ suggests that the corresponding numerical RG trajectories should display the same γ -independence. Moreover, since these fixed points originate from exact scaling solutions, they are expected to be robust under extensions of the truncation.

Finally, the appearance of exact scaling solutions $u = u_*$ and $f = f_{0*} + f_{1*}x$ and the associated fixed-point structure is not specific to the proper-time flow, see e.g. [67, 69].

B Critical exponents

Replacing the fixed-point values into the critical condition in Eq. (III.12), we find that only the fixed points in the second class can satisfy it. Since we require $f_1 > 0$, only the solution with the plus sign in Eq. (IV.5) remains. If this fixed point governs the ultraviolet (UV) regime, it can yield asymptotically free solutions for λ . Whether this happens depends on the spectrum of critical exponents.

We linearize the beta functions around the fixed point h_{i*} by perturbing the running couplings according to

$$h_i(t) = h_{i*} + e^{-t\theta} \delta h_i, \quad (\text{IV.7})$$

where $h_i \in \{u_0, x_0, \lambda, g, f_1, w\}$ and θ denotes a critical exponent. For the fixed point eq. (IV.5) with the plus sign we find a set of critical exponents that contains the canonical values $\theta = 0$, $\theta = 2$, and $\theta = 4$, as well as two additional non-trivial exponents, denoted by θ_5 and θ_6 , which depend on w_* . Figures 4(a) and 4(b) show θ_5 and θ_6 as functions of w_* for representative values of N . The exponent θ_5 is always positive and typically of order $\theta_5 \simeq 2$. By contrast, θ_6 crosses zero at a value $w_* = \bar{w}_*(N)$. For instance, for $N = 4$ one finds $\theta_6 > 0$ for $w_* \gtrsim 0.6$. In the

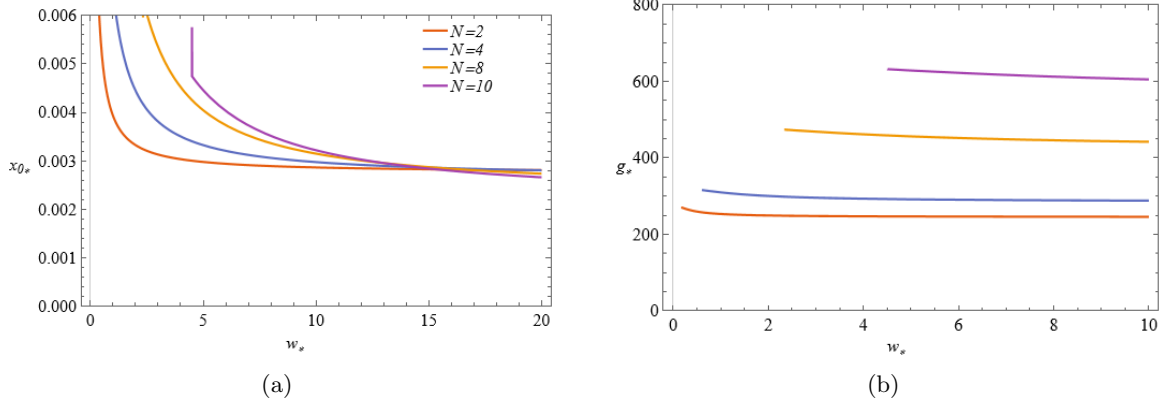


FIG. 1. Fixed-point values for the family with $f_{1*} = 1/3$, shown for $m = d/2 + 1$ and $\gamma = 1$ as functions of $w_* = a$ for representative values of N . (a) x_{0*} versus w_* . (b) g_* versus w_* .

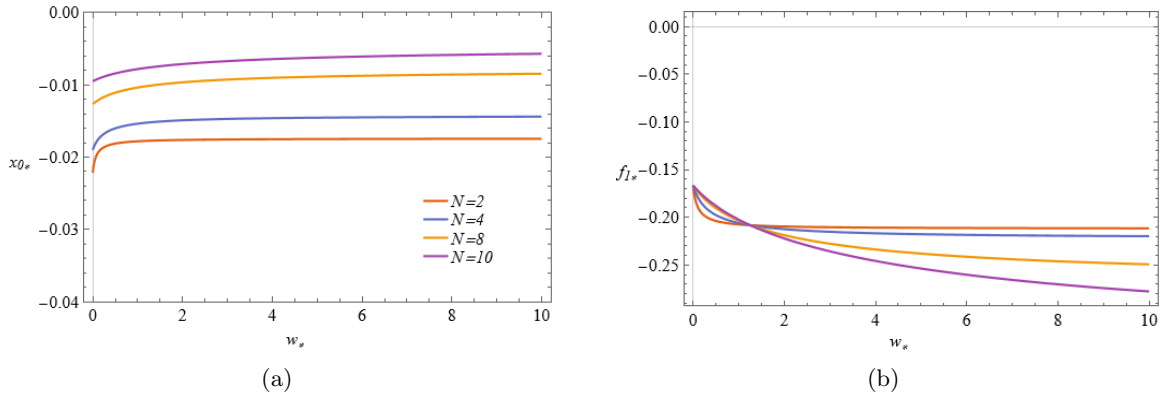


FIG. 2. Fixed-point values for the family defined by Eq. (IV.5) with the minus sign, shown for $m = d/2 + 1$ and $\gamma = 1$ as functions of $w_* = a$ for representative values of N . (a) x_{0*} versus w_* . (b) f_{1*} versus w_* .

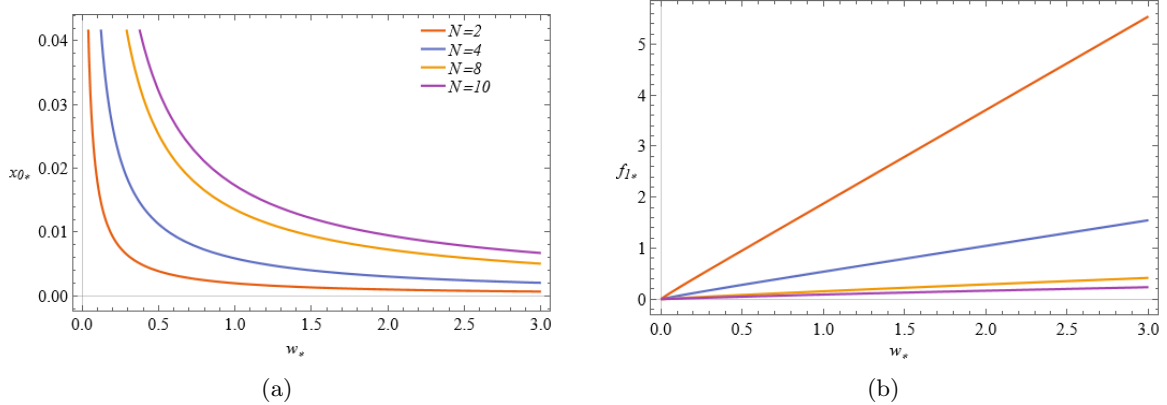


FIG. 3. Fixed-point values for the family defined by Eq. (IV.5) with the plus sign, shown for $m = d/2 + 1$ and $\gamma = 1$ as functions of $w_* = a$ for representative values of N . (a) x_{0*} versus w_* . (b) f_{1*} versus w_* .

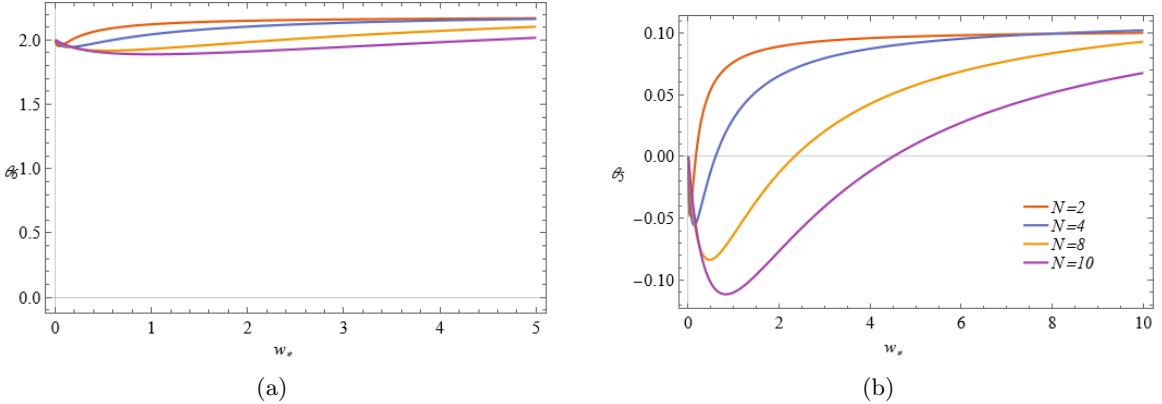


FIG. 4. Nontrivial critical exponents θ_5 and θ_6 associated with perturbations of the fixed point (IV.5) (plus-sign branch), shown as functions of w_* for representative values of N . (a) $\theta_5(w_*)$. (b) $\theta_6(w_*)$. While θ_5 remains positive, θ_6 changes sign at $w_* = \bar{w}_*(N)$.

following we focus on the parameter region $w_* > \bar{w}_*(N)$, for which both non-trivial exponents are positive and the fixed point is UV-attractive in all directions relevant for the UV completion mechanism discussed in Sec. III.

Inspecting the corresponding eigenvectors, the exponent $\theta = 4$ is associated with the u_0 direction, whereas the remaining eigendirections are non-trivial superpositions in the $(x_0, \lambda, g, f_1, w)$ subspace. Nevertheless, their projections show that the most relevant deformation has a dominant component along the Newton coupling g . This indicates that the UV scaling regime is largely controlled by the gravitational sector. The marginal and near-marginal eigendirections are also dominated by the gravitational sector but with subleading admixtures of λ and f_1 . In particular, the fixed point breaks the classical marginality of f_1 and renders it relevant. At linear order, λ is marginal in the fixed-point regime; beyond linear order it acquires logarithmic corrections, corresponding to a marginally (ir)relevant behavior. In the parameter region $w_* > \bar{w}_*(N)$, the fixed point is UV-attractive in the sense required for the UV completion mechanism described above. Since the existence of the plus-sign fixed point requires $N > 1$, the singularity can be removed only for an $O(N)$ multiplet with at least two scalar fields.

From the beta functions in Appendix B, the anomalous dimension η_L also contributes to the breaking of classical marginality. However, our qualitative conclusions do not hinge on these contributions: setting $Z_L = Z_T = 1$ leaves the fixed-point mechanism and the associated relevance properties unchanged. The breaking of marginality is thus a genuine feature of the fixed point.

The RG flow on the UV critical surface spanned by the UV fixed point yields definite pre-

dictions for the infrared (IR) values of couplings at a reference scale $t = t_0$. In practice, the projection of the UV critical surface onto the IR hyperplane spanned by $(x_0(t_0), \lambda(t_0), g(t_0), f_1(t_0))$ partitions the space of IR initial conditions into two regions, which we denote by M_1 and M_2 . Initial conditions in M_1 correspond to trajectories that remain regular for all scales and are attracted to the UV fixed point: for these trajectories gravitational fluctuations overcome matter fluctuations around the Planck scale and the conditions in Sec. III are satisfied, yielding UV-complete theories. By contrast, initial conditions in M_2 lie outside the basin of attraction of the UV fixed point: matter fluctuations continue to dominate above the Planck scale, the conditions in Eq. (III.12) and $|A| > B\lambda$ are not met, and the flow develops a Landau-pole-like singularity in the UV. Accordingly, points in M_2 correspond to trajectories that cannot be connected to the UV fixed point.

Since matter fluctuations dominate in the deep IR, following UV-complete trajectories towards $t \rightarrow -\infty$ typically brings them close to the Gaussian regime. As at the Gaussian fixed point f_1 is a free parameter, there exists a continuous family of RG trajectories connecting the Gaussian regime to the interacting UV fixed point.

V NUMERICAL ANALYSIS TO DETERMINE THE CRITICAL LINE

Determining the manifolds M_1 and M_2 requires a numerical analysis. As in the fixed-point discussion, we use $\gamma = 1$ for illustration. We solve the coupled beta functions for the running couplings $(u_0, x_0, \lambda, g, f_1, w)$ given in Appendix B, at fixed N and m . As boundary conditions we specify the couplings at $t = 0$, corresponding to $\Lambda = \Lambda_0$, i.e. the reference scale at which the IR parameters are defined, and integrate towards increasing RG time (towards the UV).

Trajectories that develop a singularity (belonging to M_2) terminate at a finite RG time $t = t_{\text{pole}}$, defined operationally as the smallest value of t at which the flow becomes singular (e.g. by a divergence of a coupling or by a vanishing denominator in the beta functions). This induces a separating surface in the space of initial conditions, which we may schematically represent as

$$0 = S(t_{\text{pole}}; x_0(0), \lambda(0), g(0), f_1(0), w(0)), \quad (\text{V.1})$$

where S encodes the condition that a singularity is reached at t_{pole} . In the purely scalar limit $f_1(0) = 0$ one recovers the standard one-loop behavior $\lambda^{-1}(t) = \lambda^{-1}(0) + \beta_0 t$, which implies a divergence at a finite t_{pole} for $\lambda(0) > 0$ and S reduces to $S = 1 + \beta_0 \lambda(0) t_{\text{pole}} = 0$ with $\beta_0 < 0$. For $f_1(0) \neq 0$, the existence of the UV-attractive fixed point discussed in Sec. IV implies that there

are initial conditions for which $\lambda(t)$ remains regular for all t and flows to $\lambda_* = 0$. Accordingly, the set of initial conditions that develop a singularity forms a bounded region in the coupling space, separated from the regular region by a critical surface.

To visualize this critical surface, we fix $(x_0(0), g(0), w(0))$ and explore the plane of initial conditions $(f_1(0), \lambda(0))$. In this two-dimensional slice, the separating surface reduces to a critical line, which we parametrize as

$$\lambda(0) = h(f_1(0)). \quad (\text{V.2})$$

We then repeat this analysis by varying $x_0(0)$, $g(0)$, and $w(0)$ one at a time, and subsequently scanning also over m and N .

To avoid numerical instabilities close to the divergence in RG time, we reparametrize the flow by using λ as the evolution parameter. Concretely, we form ratios such as

$$\frac{dx_0}{d\lambda} = \frac{\dot{x}_0}{\dot{\lambda}}, \quad \frac{dg}{d\lambda} = \frac{\dot{g}}{\dot{\lambda}}, \quad \frac{df_1}{d\lambda} = \frac{\dot{f}_1}{\dot{\lambda}}, \quad \frac{dw}{d\lambda} = \frac{\dot{w}}{\dot{\lambda}}, \quad (\text{V.3})$$

and solve the resulting system with initial conditions $x_0(\lambda(0)) = x_0(0)$, $g(\lambda(0)) = g(0)$, $f_1(\lambda(0)) = f_1(0)$, $w(\lambda(0)) = w(0)$. For a fixed value of $f_1(0)$ we then scan over $\lambda(0)$ and determine whether the solution reaches $\lambda \rightarrow \infty$ at finite t or instead remains regular and flows towards the UV fixed point. The critical value $\lambda(0) = h(f_1(0))$ is identified as the boundary between these behaviors. Repeating this procedure for a range of $f_1(0)$ yields the full curve $\lambda(0) = h(f_1(0))$. The region enclosed by this curve corresponds to the initial conditions for which $\lambda(t)$ becomes asymptotically free in the UV; it is the projection of M_1 onto the $(f_1(0), \lambda(0))$ plane at fixed $(x_0(0), g(0), w(0))$. An example of such a projection is shown in Fig. 5(a).

In our analysis we find that the value of $x_0(0)$ has no appreciable impact on the critical line $\lambda(0) = h(f_1(0))$. Figure 5(b) shows $\lambda(0) = h(f_1(0))$ for $m = d/2 + 1$, $N = 4$, $(x_0(0), w(0)) = (0.1, 1)$ and several values of $g(0)$ chosen near the Gaussian regime $g_* = 0$. The curves exhibit a single maximum and decay to $\lambda(0) \rightarrow 0$ as $f_1(0) \gg 1$. As $g(0)$ increases, the maximum shifts to larger values of $\lambda(0)$. A similar behavior is observed when fixing $g(0)$ and varying $w(0)$: Fig. 6(a) shows the critical line for different values of $w(0)$ at fixed $g(0)$ and $x_0(0)$. Varying the number of scalar fields N also yields a similar qualitative behavior, as shown in Fig. 6(b).

Finally, varying the cutoff-shape parameter m at fixed initial conditions and fixed N , we find only a mild dependence of the critical line on m . This is illustrated in Fig. 7(a), which shows

the logarithm of the absolute difference

$$\delta(h, X) = |h(f_1(0); m = 3) - h(f_1(0); m = X)| \quad (\text{V.4})$$

for several values X as a function of $f_1(0)$ (with $\gamma = 1$). This indicates that the existence and qualitative shape of the critical line are not artifacts of the parameter m .

The same analysis can be performed for the second cutoff family $\gamma = m$. For identical initial conditions and the same values of m and N , we find that the critical line $\lambda(0) = h(f_1(0))$ is insensitive to the choice of γ . This is shown in Fig. 7(b), where we plot

$$\delta(h, \gamma) = |h(f_1(0); \gamma = m) - h(f_1(0); \gamma = 1)| \quad (\text{V.5})$$

as a function of $f_1(0)$ for several values of $g(0)$. We therefore conclude that the critical line $\lambda(0) = h(f_1(0))$ is not an artifact of the cutoff family.

In all plots the critical line starts at a minimum value $f_{1,\min}(0)$ for which $\lambda(0) = 0$. This threshold depends only on N and $w(0)$. For $f_1(0)$ slightly above $f_{1,\min}(0)$, the critical line rises approximately linearly in $f_1(0) - f_{1,\min}(0)$, with a slope that depends on $(g(0), w(0), N)$. After reaching a maximum, the curve enters an asymptotic regime in which it decays as

$$\lambda(0) = \frac{\gamma g_* f_{1*} w_*^2}{12(m-1)} \frac{1}{f_1(0)} \quad \text{for } f_1(0) \gg 1. \quad (\text{V.6})$$

in this regime there is no dependence on the initial conditions of $g(t)$, $x_0(t)$ and $w(t)$. Additionally, there is also no dependence on m since $g_* = \frac{192\pi^2(m-1)}{(16-N)\gamma}$, so the critical line is cutoff independent for $f_1(0) \rightarrow \infty$. Also, in this limit, at fixed N , all critical lines focus into a single line, this is shown in the inset of fig. 5(b).

Now we briefly recast the previous results in geometric terms, which also clarifies the origin of the asymptotic relation eq. (V.6). The RG flow defines a vector field on the coupling space,

$$\dot{\mathbf{g}}(t) = \beta(\mathbf{g}), \quad \mathbf{g}(t) = (x_0(t), \lambda(t), g(t), f_1(t), w(t)), \quad (\text{V.7})$$

whose integral curves are the RG trajectories. Let \mathbf{g}_* denote the UV fixed point in eq.(IV.5) (with the plus sign). The set of initial data at $t = 0$ whose trajectories are regular for all $t \geq 0$ and satisfy $\lim_{t \rightarrow +\infty} \mathbf{g}(t) = \mathbf{g}_*$ defines the IR UV-complete manifold M_1 . Equivalently, M_1 is the intersection at $t = 0$ of the (UV) stable manifold $W^s(\mathbf{g}_*)$ of the fixed point with the IR

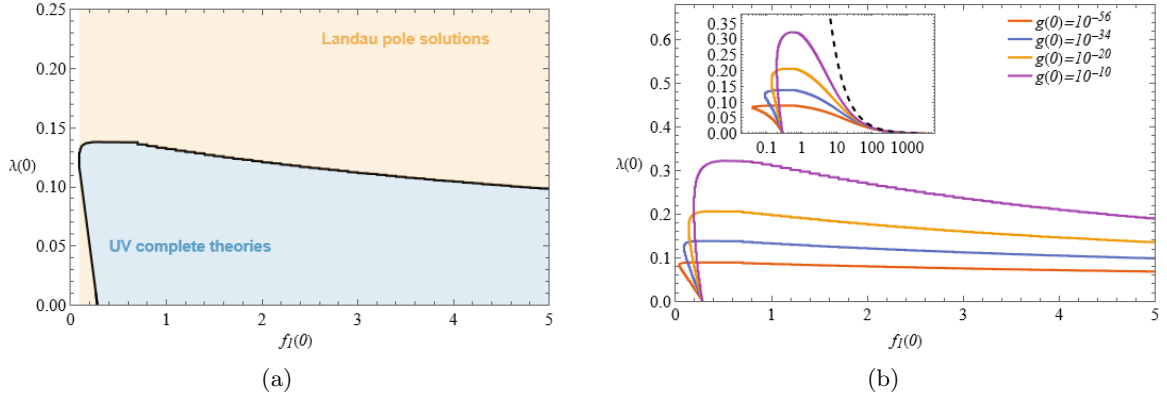


FIG. 5. Projection of the IR coupling plane $(f_1(0), \lambda(0))$ at fixed $(x_0(0), g(0), w(0))$, illustrating the separation between UV-complete and singular trajectories. (a) Example for $g(0) = 10^{-34}$, $x_0(0) = 0.1$, $w(0) = 1$ and $N = 4$: the region corresponding to UV-complete trajectories (projection of M_1) is bounded by the critical line $\lambda(0) = h(f_1(0))$ (black). Outside this region, trajectories develop a singularity (projection of M_2). (b) The critical line $\lambda(0) = h(f_1(0))$ for several values of $g(0)$ at fixed $x_0(0)$ and $w(0)$. In the inset the full range up to $f_1(0) \rightarrow \infty$. The black dashed line is the asymptotic limit eq.(V.6).

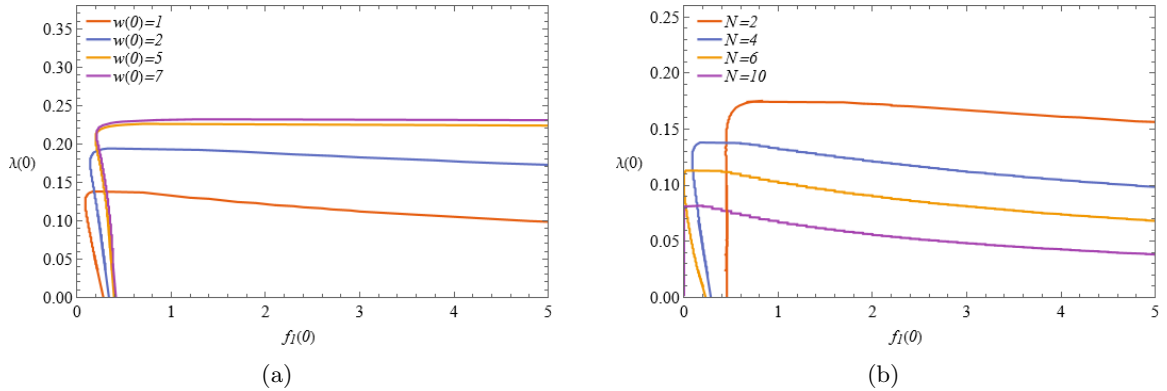


FIG. 6. Dependence of the critical line $\lambda(0) = h(f_1(0))$ on IR parameters. (a) Variation with $w(0)$ at fixed $N = 4$ and fixed $(g(0), x_0(0))$. (b) Variation with N at fixed $(g(0), x_0(0), w(0))$.

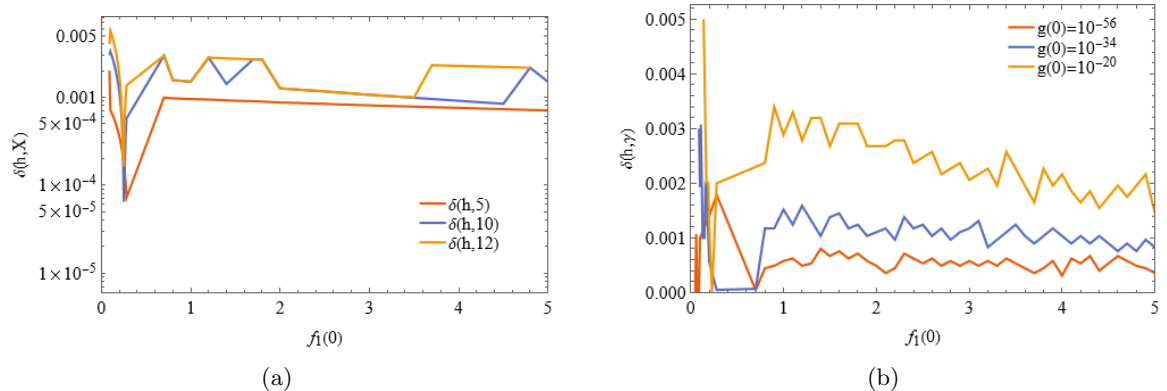


FIG. 7. Robustness of the critical line under changes of the cutoff scheme. (a) $\delta(h, X) = |h(f_1(0); m = 3) - h(f_1(0); m = X)|$ as a function of $f_1(0)$ for several values X (with $\gamma = 1$). (b) $\delta(h, \gamma) = |h(f_1(0); \gamma = m) - h(f_1(0); \gamma = 1)|$ as a function of $f_1(0)$ for several values of $g(0)$, comparing the two cutoff families $\gamma = 1$ and $\gamma = m$.

hyperplane.

Locally, M_1 can be described as the zero level-set of a function $S_{\text{reg}}(\mathbf{g})$,

$$S_{\text{reg}}(\mathbf{g}) = 0, \quad (\text{V.8})$$

and the defining property of such an invariant manifold is that the RG vector field is tangent to it. Denoting by $\mathbf{n}(\mathbf{g}) = \nabla S_{\text{reg}}(\mathbf{g})$ the normal to the hypersurface, tangency is expressed by

$$0 = \mathbf{n} \cdot \boldsymbol{\beta} = \sum_i (\partial_{g_i} S_{\text{reg}}) \beta_{g_i}, \quad g_i \in \{x_0, \lambda, g, f_1, w\}. \quad (\text{V.9})$$

Selecting λ as a representative coupling, one may equivalently parameterize the manifold as

$$S_{\text{reg}}(\mathbf{g}) = \lambda - \lambda_{\text{reg}}(x_0, g, f_1, w) = 0, \quad (\text{V.10})$$

so that eq. (V.9) becomes a first-order condition determining λ_{reg} along the RG characteristics.

In the large- $f_1(0)$ regime at fixed N , the UV-complete trajectories rapidly approach the fixed-point values of the remaining couplings, $(x_0, g, w) \rightarrow (x_{0*}, g_*, w_*)$, while $f_1(0)$ acts as an external large parameter in the projection to the $(f_1(0), \lambda(0))$ plane. To leading order, the tangency condition eq. (V.9) therefore reduces to the requirement that the λ -component of the flow vanishes on the asymptotic trajectory ²,

$$\beta_\lambda \left(x_{0*}, \frac{\lambda(0)}{2}, g_*, f_1(0), w_* \right) = 0. \quad (\text{V.11})$$

Solving this equation for $\lambda(0)$ and expanding for $f_1(0) \rightarrow \infty$ yields precisely the asymptotic critical line eq. (V.6), explaining why, at fixed N , the numerical critical lines collapse onto a single curve in that limit (cf. the inset of Fig. 5(b)).

VI NUMERICAL SOLUTIONS

A Numerical runnings

The flow equations in Appendix B can be solved only numerically. Eliminating t from the solutions, one can construct RG trajectories in the five-dimensional coupling space $(x_0, \lambda, g, f_1, w)$ or equivalently the hypersurface S_{reg} . Since these trajectories cannot be visualized in the full space, we show representative projections of S_{reg} . In particular, the projection onto the (f_1, λ)

² In eq. (V.11) the coupling λ is replaced by $\lambda(0)/2$ and not simply by $\lambda(0)$ due to the Taylor expansion of $u_t(x)$.

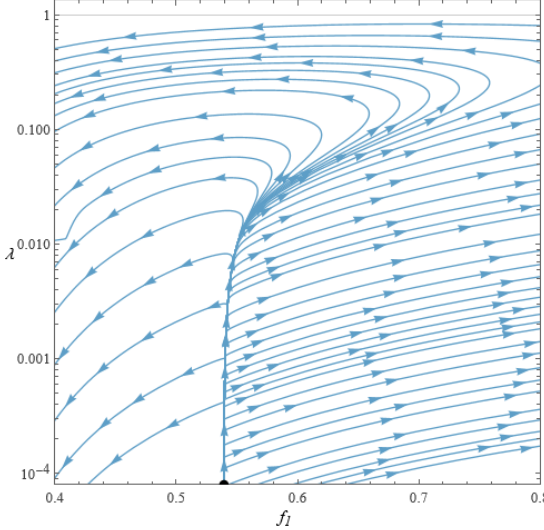


FIG. 8. Projection of representative RG trajectories onto the (f_1, λ) plane for $t \gtrsim t_{\text{tr}}$ (Planck and UV regime), obtained from initial conditions inside the UV-complete region. The example shown uses $N = 4$, $g(0) = 10^{-56}$, $w(0) = 1$ and $x_0(0) = 1$. Arrows indicate the direction of decreasing RG time (from UV to IR). In the Planck regime gravitational fluctuations induce a turnaround: instead of growing monotonically, both λ and f_1 reach a maximum and then decrease towards the UV fixed point (IV.5). For $w(0) = 1$ one finds $f_{1*} \approx 0.539$, marked by the black dot.

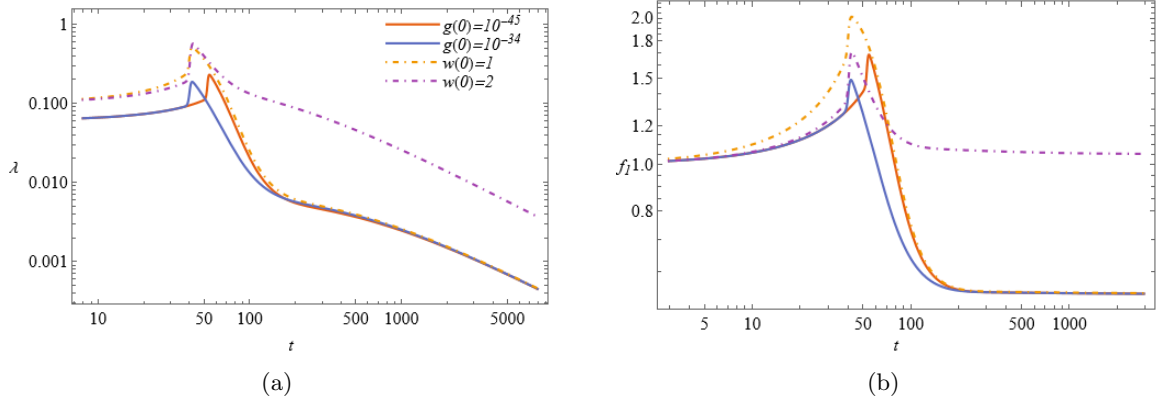


FIG. 9. Representative UV-complete runnings for $N = 4$. (a) Running of $\lambda(t)$. (b) Running of $f_1(t)$. Solid lines: different values of $g(0)$ at fixed $w(0)$ and $x_0(0)$. Dot-dashed lines: different values of $w(0)$ at fixed $g(0)$ and $x_0(0)$.

plane for scales above the Planck regime is shown in Fig. 8. For initial conditions inside the UV-complete region (the projection of M_1 in Fig. 5(a)), all trajectories approach the interacting UV fixed point.

The RG-time evolution of representative UV-complete trajectories for $N = 4$ is shown in Figs. 9(a) and 9(b). Solid lines correspond to solutions at fixed $w(0)$ and $x_0(0)$ for two different values of $g(0)$, namely $g(0) = 10^{-45}$ and $g(0) = 10^{-34}$. Dot-dashed lines correspond to solutions

at fixed $g(0)$ and $x_0(0)$ for two different values of $w(0)$, namely $w(0) = 1$ and $w(0) = 2$. The running $\lambda(t)$ follows the matter-dominated (Gaussian) behavior up to a transition value

$$t_{\text{tr}} \sim \ln\left(\frac{m_p}{\Lambda_0}\right), \quad (\text{VI.1})$$

at which gravitational fluctuations become important and $g(t)$ crosses over from the Gaussian regime to the non-Gaussian fixed-point regime. Around this crossover, $\lambda(t)$ reaches a maximum and subsequently decreases towards $\lambda_* = 0$, with an asymptotic behavior compatible with $\lambda(t) \sim 1/t$ at large t . The running of $f_1(t)$ shows a similar crossover and approaches its fixed-point value f_{1*} in the UV.

The transition scale is where the critical condition eq.([III.12](#)) starts to be satisfied. Indeed, the maximum of $\lambda(t)$ corresponds to a zero of the beta function β_λ . This is exactly where the condition $\lambda_* = A_*/B_*$ of Sec. [III](#) holds and then for larger t the inequality $|A(t)| > B(t)\lambda(t)$ is satisfied, allowing the decreasing of $\lambda(t)$. In particular, in the limit $t = +\infty$ eq.([III.12](#)) gives the constraint $1/g_* = f_{1*}x_{0*}$, which eq.([IV.5](#)) satisfies, and the running of f and u reduces to $f(t \rightarrow \infty) = f_{1*}x$ and $u(t \rightarrow \infty) = u_{0*}$ reproducing the exact scaling solution.

In all cases, the running of $g(t)$ shown in Fig. [10\(a\)](#) is qualitatively similar to the pure-gravity behavior: a Gaussian regime at low scales crosses over to the non-Gaussian scaling regime around t_{tr} . The running of $x_0(t)$, shown in Fig. [10\(b\)](#), exhibits two quasi-constant regimes; the second is approached in the non-Gaussian fixed-point regime of Eq. ([IV.5](#)). In particular, the system remains in the symmetry-broken phase along the displayed trajectories.

Figures [11\(a\)](#) and [11\(b\)](#) show the anomalous dimensions $\eta_L(t)$ and $\eta_T(t)$. Both remain small but non-vanishing. As for $\lambda(t)$, they develop a peak around the crossover to the non-Gaussian regime and then decay slowly towards their fixed-point values $\eta_{L*} = 0$ and $\eta_{T*} = 0$. Due to the smallness of $\eta_{L,T}$, the ratio $w(t)$ in Figs. [12\(a\)](#) and [12\(b\)](#) is nearly constant over the full RG interval. Deviations from the IR value $w(0)$ start around t_{tr} , after which $w(t)$ approaches its UV value. The initial conditions thus fix the free parameter w_* of the UV fixed point eq. ([IV.5](#)), which in turn determines the corresponding fixed-point values $x_{0*}(w_*)$ and $f_{1*}(w_*)$.

Changing $g(0)$ at fixed $w(0)$ and $x_0(0)$ primarily affects the length of the matter-dominated regime: the smaller $g(0)$ is, the longer the trajectory stays close to the Gaussian regime before crossing over. The location of the maximum in λ and f_1 shifts accordingly, while the UV scaling behavior is essentially unchanged. By contrast, changing $w(0)$ at fixed $g(0)$ and $x_0(0)$ mainly

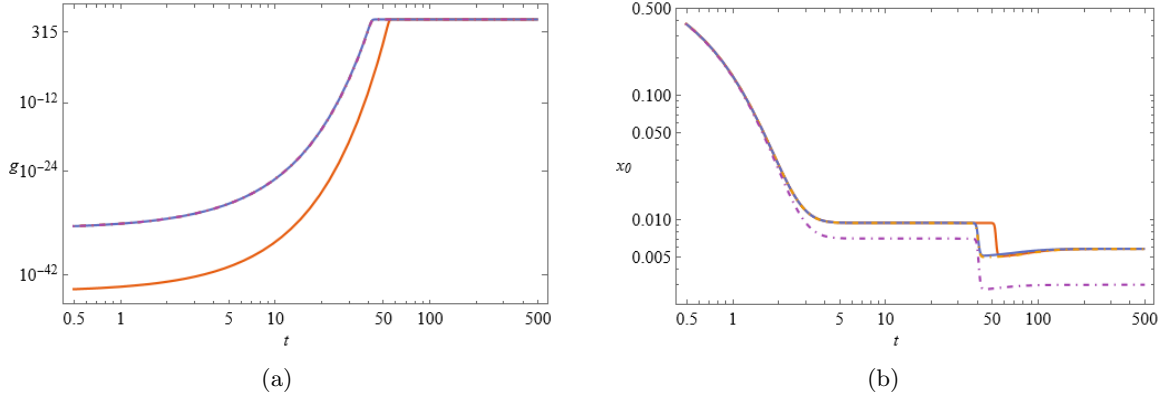


FIG. 10. Representative UV-complete runnings for $N = 4$. (a) Running of $g(t)$, showing the crossover from the Gaussian regime to the non-Gaussian scaling regime around t_{tr} . (b) Running of $x_0(t)$, which approaches a quasi-constant value in the fixed-point regime of Eq. (IV.5).

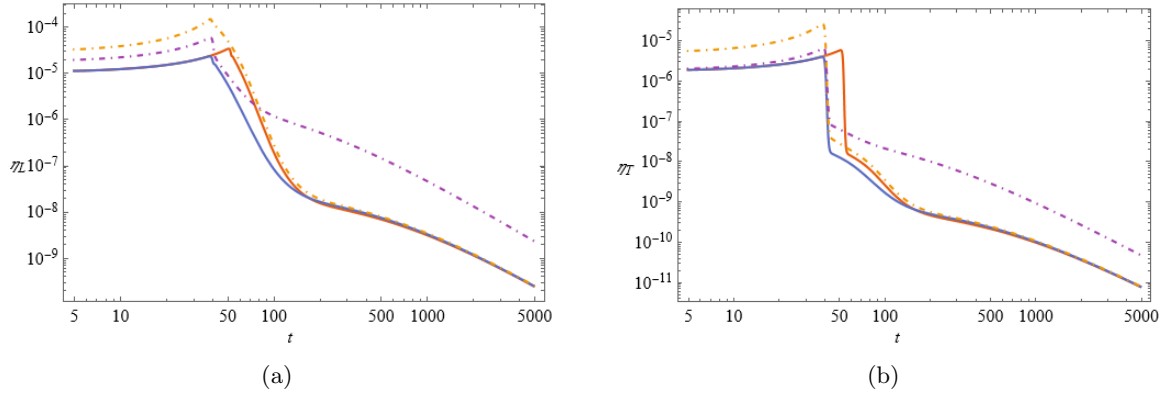


FIG. 11. Representative UV-complete runnings for $N = 4$. (a) Running of $\eta_L(t)$. (b) Running of $\eta_T(t)$. Both anomalous dimensions peak around the crossover and then decay slowly towards $\eta_{L*} = 0$ and $\eta_{T*} = 0$

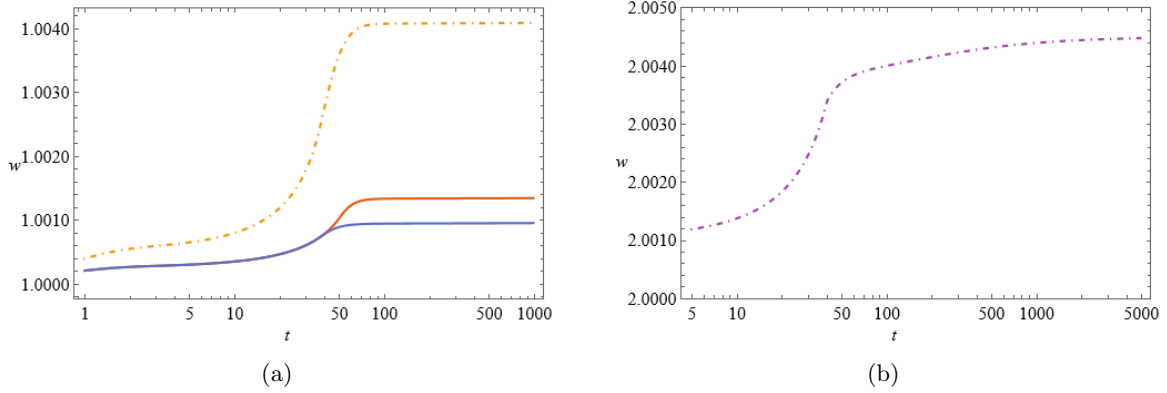


FIG. 12. Representative UV-complete runnings for $N = 4$. (a) Running of $w(t)$ for a solution with $w(0) = 1$. (b) Running of $w(t)$ for a solution with $w(0) = 2$. In both cases $w(t)$ stays close to $w(0)$ in the Gaussian regime and approaches its UV value after the crossover. The IR initial conditions fix the free parameter w_* of the UV fixed point eq.(IV.5).

affects the UV scaling regime and its approach to the fixed point. While $g(t)$ depends only weakly on $w(0)$, the maxima of $\lambda(t)$ and $f_1(t)$, as well as the asymptotic coefficients in the large- t expansions (e.g. $\lambda(t) \sim 1/t + O(1/t^2)$), show a pronounced dependence on $w(0)$. This is reflected in the different numerical values of $x_{0*}(w_*)$ and $f_{1*}(w_*)$ approached in the UV.

B Limits on the mass of the scalar

The independence of the critical line $\lambda(0) = h(f_1(0))$ from m and γ allows us to extract predictions that are insensitive to the cutoff choice. In particular, it can be used to constrain the scalar mass in the broken phase, cf. Eq. (III.4), evaluated at the reference scale $t = 0$. To extract a definite value at $t = 0$ we adopt a naturalness-motivated assumption [70] and set the vacuum expectation value to be of the same order as the measurement scale Λ_0 , i.e ³

$$x_0(t = 0) = Z_L(\Lambda_0) \frac{\rho_0}{\Lambda_0^2} = 1, \quad (\text{VI.2})$$

so that the mass constraint can be expressed directly in terms of IR parameters.

At the reference scale, the Planck mass is related to $g(0)$ by

$$g(0) = \frac{\Lambda_0^2}{m_p^2}, \quad (\text{VI.3})$$

where $m_p \simeq 10^{19}$ GeV. Figure 13(a) illustrates how the projection of the IR critical manifold constrains the scalar mass at fixed $g(0)$, $w(0)$ and N . In this representation, the critical line in the $(f_1(0), \lambda(0))$ plane becomes a *critical mass line* in the $(f_1(0), m_\sigma(0))$ plane: as in the previous discussion, the region below the curve corresponds to UV-complete trajectories, while points above it lead to Landau-pole-like behavior. The critical mass line exhibits a maximum and then decreases at large $f_1(0)$. In the asymptotic limit $f_1(0) \gg 1$, using eq.(V.6) we get

$$m_{\sigma, \text{crit}}(f_1(0) \rightarrow \infty) = \frac{m_p(0)}{3} \sqrt{\frac{\gamma g_* f_{1*}}{2(m-1)(N-1)}} w_* \left(\frac{1}{f_1(0)} \right)^{3/2} + O \left(\frac{1}{f_1(0)} \right)^{5/2} \quad (\text{VI.4})$$

replacing the fixed point value $g_* = \frac{192\pi^2(m-1)}{(16-N)\gamma}$ shows that this expression does not depend on m , as for the asymptotic of the critical line. Furthermore, in this asymptotic limit, all critical mass lines focus on a single critical mass line.

Figure 13(b) shows the critical mass line as a function of $f_1(0)$ for $N = 4$ and several values of

³ In this context, “naturalness” refers to the expectation that IR observables should not depend sensitively on UV physics without an additional mechanism (such as a symmetry). In particular, gravitational fluctuations are expected to decouple from the dynamics for $\Lambda \ll m_p$.

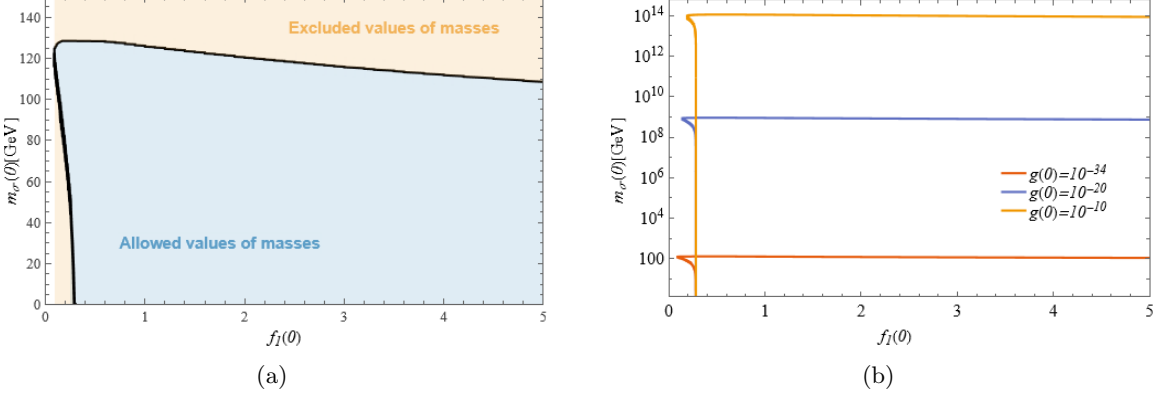


FIG. 13. Constraints on the scalar mass from the UV-complete region in the $(f_1(0), m_\sigma(0))$ plane. (a) Example at $g(0) = 10^{-34}$, $x_0(0) = 1$, $w(0) = 1$ and $N = 4$: the light-blue region corresponds to the projection of the IR critical manifold M_1 (UV-complete trajectories), while the beige region corresponds to singular trajectories. The black curve is the critical mass line separating the two behaviors. (b) Same as (a), shown for several values of $g(0)$ (logarithmic scale).

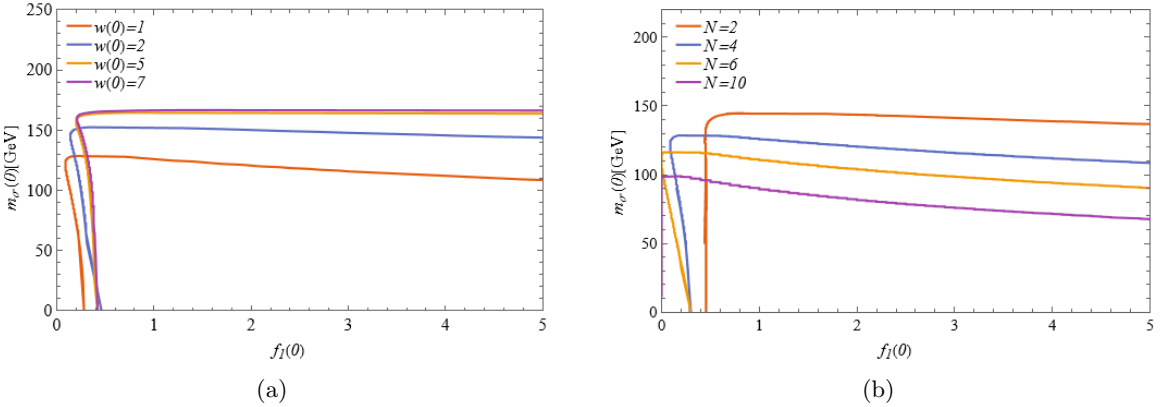


FIG. 14. Dependence of the critical mass line on IR parameters. (a) Variation with $w(0)$ at fixed $N = 4$ and fixed $(g(0), x_0(0))$. (b) Variation with N at fixed $(g(0), x_0(0), w(0))$.

$g(0)$. The allowed mass range depends strongly on $g(0)$, changing by many orders of magnitude as $g(0)$ is varied. By contrast, at fixed $g(0)$, the dependence on $w(0)$ (Fig. 14(a)) and on N (Fig. 14(b)) is milder, and the resulting mass range typically remains within the same order of magnitude.

The maximum allowed scalar mass is determined by the peak of the critical line, i.e. by the pair $(\bar{f}_1(0), \lambda_{\max}(0))$ with $\lambda_{\max}(0) = h(\bar{f}_1(0))$. In $d = 4$, at $t = 0$, one finds

$$m_{\sigma,\max}(t = 0) = 2\Lambda_0 \sqrt{\frac{\lambda_{\max}(0) x_0(0)}{1 + 6 \bar{f}_1^2(0) x_0(0) g(0)}}. \quad (\text{VI.5})$$

This expression makes the strong sensitivity to $g(0)$ explicit. Expanding around $g(0) = 0$

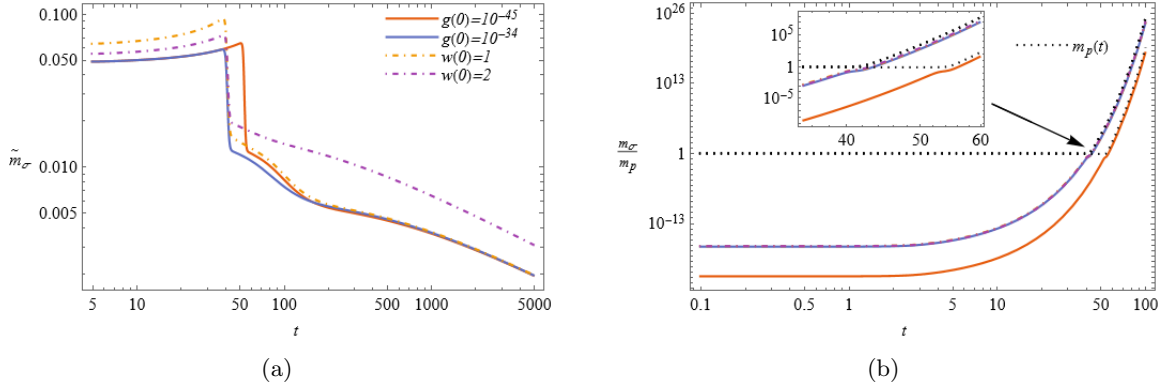


FIG. 15. Running of the longitudinal scalar mass for the four solutions discussed in the subsection VI A. In (a) the running of dimensionless mass. In (b) the running of dimensionfull mass in unit of Plank mass. The zoom around the transition scale highlights the change of scaling behavior from $m_\sigma(t) \sim m_\sigma(0)e^t$ to $\sim m_\sigma(0)t^{-1/2}e^t$. The black dotted lines show the running of Plank mass. Above the transition scale there is no distinction between the running of m_p and m_σ .

yields $m_{\sigma,\max}(t=0) = 2\Lambda_0\sqrt{x_0(0)\lambda_{\max}(0)} + O(g(0))$. Since $\Lambda_0^2 = m_p^2 g(0)$, the overall scale is set by the competition between the largeness of m_p and the smallness of $g(0)$. If $g(0)$ is not small enough to compensate the Planck scale, the maximum scalar mass remains parametrically below m_p ; conversely, for extremely small $g(0)$ the maximum mass becomes very small. For example, for $g(0) = 10^{-56}$ (corresponding to a measurement performed at $\Lambda_0 \sim 1$ eV) we find $m_{\sigma,\max}(t=0) \sim 10^{-10}$ GeV.

As a further illustrative example, consider $N = 4$ and a reference scale near the top-quark mass, $\Lambda_0 = m_t \simeq 173$ GeV, for which $g(0) \sim 10^{-34}$. In this case we find $\lambda_{\max}(0) \simeq 0.138$, which along with the condition $x_0(0) = 1$ gives $v \simeq Z_L(\Lambda_0)244$ GeV and then corresponds to $m_{\sigma,\max} \simeq 128.5$ GeV.

C Running of the scalar mass

We now discuss the running of the longitudinal scalar mass. Figure 15(a) shows the RG evolution of the dimensionless mass \tilde{m}_σ for the four numerical solutions introduced in Sec. VI A. For $t \ll t_{\text{tr}}$ the running is almost frozen, $\tilde{m}_\sigma(t) \simeq \tilde{m}_\sigma(0)$. Around the transition scale t_{tr} , where gravitational fluctuations start to dominate, $\tilde{m}_\sigma(t)$ develops a maximum and then crosses a short transient regime before approaching the UV fixed point value $\tilde{m}_{\sigma*} = 0$.

In the asymptotic UV regime we find a slow decay,

$$\tilde{m}_\sigma(t) \sim t^{-1/2} \quad (t \rightarrow \infty). \quad (\text{VI.6})$$

This behavior is expected: near the UV fixed point all couplings approach constant values, while the quartic coupling is marginally running as $\lambda(t) \sim 1/t$. Since at leading order $\tilde{m}_\sigma^2 \propto x_0 \lambda$ (cf. Eq. (III.4)), one obtains $\tilde{m}_\sigma(t) \propto \sqrt{\lambda(t)} \sim t^{-1/2}$.

The dependence on the IR initial conditions mirrors the behavior discussed for $\lambda(t)$ in Sec. VI A: changing $g(0)$ at fixed $w(0)$ mainly shifts the extent of the matter-dominated regime below t_{tr} , whereas changing $w(0)$ at fixed $g(0)$ primarily affects the gravity-dominated regime above t_{tr} .

Figure 15(b) shows the corresponding dimensionful mass, plotted in units of the reference Planck mass at $t = 0$. Below t_{tr} the nearly constant \tilde{m}_σ implies the canonical scaling $m_\sigma(t) \propto \Lambda \propto e^t$. Above t_{tr} the UV decay of \tilde{m}_σ induces an additional suppression, so that

$$m_\sigma(t) = \Lambda \tilde{m}_\sigma(t) \sim e^t t^{-1/2}, \quad (t \gtrsim t_{\text{tr}}). \quad (\text{VI.7})$$

In the same figure we also show the running Planck mass $m_p(t)$ (dotted curves). In the matter-dominated regime $m_p(t)$ is approximately constant, while above t_{tr} it follows the same overall scaling pattern as $m_\sigma(t)$. This can be understood from the critical relation eq. (III.12), which becomes approximately saturated above the transition and implies $x_0 \sim 1/(f_1 g)$. Inserting this into Eq. (III.4) yields the parametric estimate

$$m_\sigma(t) \sim 2 m_p(t) \sqrt{\frac{\lambda(t)}{f_1(t) (1 + 6f_1(t))}}, \quad (\text{VI.8})$$

showing that m_σ is of order m_p up to a factor $\propto \sqrt{\lambda(t)}$, and hence $m_\sigma/m_p \rightarrow 0$ as $\lambda \rightarrow 0$ in the UV.

VII CONCLUSIONS

In this work we studied an $O(N)$ scalar theory non-minimally coupled to Einstein gravity in the symmetry-broken phase. Using a polynomial truncation around the running minimum of the scalar potential, we employed the proper-time flow equation to compute the RG running of the minimum of the potential, the non-minimal coupling, the quartic coupling, and the cosmological-constant term within the truncation.

Working with the exponential parametrization and the physical gauge, we identified an interacting UV-attractive fixed point. This fixed point opens the possibility of UV-complete trajectories for the quartic scalar coupling without invoking fermionic degrees of freedom. The

fixed point is tied to an exact scaling solution of the underlying flow equation of the form $u = u_*$ and $f = f_{1*}x$ and is therefore expected to be robust under extensions of the truncation. The fixed-point value of f_{1*} lies close to the conformal value, with f_{1*} determined by Eq. (IV.5). Closely related fixed-point structures in scalar–tensor systems have also been reported within the Wetterich formalism, see e.g. [69].

The UV fixed point spans a finite-dimensional UV critical surface. Its stability spectrum contains the canonical exponents $\theta = 0$, $\theta = 2$ and $\theta = 4$, as well as additional non-trivial exponents $\theta_{5,6}$ that depend on N and on the free fixed-point parameter w_* (see Figs. 4(b) and 4(a)). The associated eigendirections are, in general, non-trivial superpositions in the space of couplings. Apart from the direction associated with u_0 (with $\theta = 4$), the most relevant deformation has a dominant projection along the Newton coupling g . This indicates that the approach to the UV fixed point is largely controlled by gravitational fluctuations. In particular, the fixed point breaks the classical marginality of f_1 and renders it relevant, while λ is marginal at linear order and acquires logarithmic corrections beyond linear order, consistent with an asymptotic behavior of the form $\lambda(t) \sim 1/t + O(1/t^2)$.

Evolving trajectories on the UV critical surface towards the infrared defines a corresponding basin of attraction in the space of IR couplings. This basin contains precisely those IR initial conditions that lead to UV-complete trajectories attracted to the UV fixed point. In practice, this separates IR initial data into two classes: one class yields regular flows for all scales and approaches the UV fixed point, while the complementary class develops a singularity at finite t . The separating boundary can be characterized numerically and, at fixed $(g(0), w(0), x_0(0), N, m)$, appears as a critical line $\lambda(0) = h(f_1(0))$ in the $(f_1(0), \lambda(0))$ plane (see Fig. 5(a)). We find that this critical line is robust under changes of the cutoff family (switching between $\gamma = 1$ and $\gamma = m$) and depends only mildly on the cutoff-shape parameter m . Its dependence on $x_0(0)$ is also weak, while the strongest dependence is on $g(0)$, $w(0)$ and N , in line with the fact that the UV scaling regime is strongly influenced by the g -direction.

The critical line provides a practical UV-completion criterion: for given $(g(0), w(0))$, UV-complete trajectories correspond to IR values $(f_1(0), \lambda(0))$ lying in the region bounded by $\lambda(0) = h(f_1(0))$. Adopting the naturalness-motivated choice $x_0(0) = 1$ allows us to translate this constraint into bounds on the physical mass of the longitudinal mode $m_\sigma(t = 0)$ via Eq. (III.4). Interestingly enough, the peak of the critical line determines an upper bound $m_{\sigma,\max}(t = 0)$ for fixed $g(0)$ and N . For illustrative choices of Λ_0 in the vicinity of the electroweak scale, the

resulting upper bounds can lie in the $\mathcal{O}(10^2 \text{ GeV})$ range.

An important next step is to extend the present framework to more realistic matter sectors. Including gauge fields and fermions introduces additional fluctuation channels that feed into the running of the scalar potential and of the non-minimal coupling. In particular, gravitational fluctuations are known to favor antiscreening contributions in Abelian gauge sectors, suggesting that the mechanism identified here may persist in the presence of gauge interactions and could potentially be relevant for curing Landau-pole behavior in Abelian theories. At the same time, Yukawa interactions provide a competing contribution to the scalar self-coupling and can shift the UV behavior of λ . It will therefore be important to determine whether the UV-attractive fixed point characterized here by $f_{1*} > 0$ and $\lambda_* = 0$ survives once gauge and Yukawa couplings are included, and to map the resulting UV-complete region in the enlarged theory space.

ACKNOWLEDGEMENTS

We thank Andrea Spina Gabriele Giacometti for useful discussions, and Dario Zappal'a and Giampaolo Vacca for comments on the manuscript. A.B. is grateful to Holger Gies for enlightening discussions on and to the Physics Department of the University of Jena for hospitality.

Appendices

A DERIVATION OF THE FLOW EQUATIONS FOR Z_L AND Z_T

In this appendix we derive the proper-time flow equations for the running wave-function renormalizations $Z_L(\Lambda)$ and $Z_T(\Lambda)$ entering Eq. (II.1). We build on the background-field and heat-kernel setup of Ref. [66].

A Projection on the kinetic operators

To extract $\Lambda\partial_\Lambda Z_T(\Lambda)$ and $\Lambda\partial_\Lambda Z_L(\Lambda)$ we project the flow on the operators $\phi_a(-\square)\phi_a$ ($a = 1, \dots, N-1$) and $\phi_N(-\square)\phi_N$, respectively. Since we are projecting on the scalar kinetic terms, only the scalar block of the Hessian is required. The projection reads

$$\int d^d x \sqrt{g} \left[\frac{1}{2} (\Lambda\partial_\Lambda Z_T) \sum_{a=1}^{N-1} \phi_a(-\square)\phi_a + \frac{1}{2} (\Lambda\partial_\Lambda Z_L) \phi_N(-\square)\phi_N \right] = \frac{1}{2} \int_0^\infty \frac{ds}{s} r(s, \Lambda^2 \mathbf{Z}) \text{Tr} \left[e^{-sS_{\Phi\Phi}^{(2)}} \right], \quad (\text{A.1})$$

where $S_{\Phi\Phi}^{(2)}$ denotes the scalar block of the Hessian, \mathbf{Z} the corresponding matrix of kinetic prefactors, and Tr includes the functional trace and the internal $O(N)$ trace.

The scalar Hessian can be written as (see Ref. [66])

$$S_{\Phi\Phi}^{(2)} = \int d^d x \sqrt{g} \frac{1}{2} \Phi^a H_{ab}(\rho) \Phi^b, \quad H_{ab}(\rho) = -Z_{ab} \square + E_{ab}, \quad (\text{A.2})$$

with

$$Z_{ab} = \begin{cases} Z_T(\Lambda) & a = b \neq N \\ Z_L(\Lambda) + 4\bar{\rho} \frac{d-1}{d-2} \frac{[F'(\bar{\rho})]^2}{F(\bar{\rho})} & a = b = N \\ 0 & a \neq b \end{cases} \quad (\text{A.3})$$

and

$$E_{ab} = \left(2\bar{\rho} U''(\bar{\rho}) + U'(\bar{\rho}) - \left[2\bar{\rho} F''(\bar{\rho}) + F'(\bar{\rho}) - \frac{4\bar{\rho}}{d-2} \frac{[F'(\bar{\rho})]^2}{F(\bar{\rho})} \right] \bar{R} \right) P_{ab}^L + \left(U'(\bar{\rho}) - F'(\bar{\rho}) \bar{R} \right) P_{ab}^T. \quad (\text{A.4})$$

Here a bar denotes evaluation on the background, and P_{ab}^L and P_{ab}^T are the longitudinal (radial) and transverse projectors defined in the main text.

It is convenient to introduce the longitudinal and transverse “mass” terms

$$E_{ab} = M_L(\bar{\rho}) P_{ab}^L + M_T(\bar{\rho}) P_{ab}^T, \quad (\text{A.5})$$

with

$$\begin{aligned} M_L(\bar{\rho}) &= 2\bar{\rho} U''(\bar{\rho}) + U'(\bar{\rho}) - \left[2\bar{\rho} F''(\bar{\rho}) + F'(\bar{\rho}) - \frac{4\bar{\rho}}{d-2} \frac{[F'(\bar{\rho})]^2}{F(\bar{\rho})} \right] \bar{R}, \\ M_T(\bar{\rho}) &= U'(\bar{\rho}) - F'(\bar{\rho}) \bar{R}. \end{aligned} \quad (\text{A.6})$$

B Heat-kernel expansion

We bring the operator to Laplace type by factoring out \mathbf{Z} ,

$$-\mathbf{Z}\square + \mathbf{E} = \mathbf{Z}(-\square + \mathbf{U}), \quad \mathbf{U} \equiv \mathbf{Z}^{-1}\mathbf{E}. \quad (\text{A.7})$$

In components, \mathbf{U} decomposes as

$$\mathbf{U}_{ab} = U_L P_{ab}^L + U_T P_{ab}^T, \quad U_L = \frac{M_L}{Z_{NN}}, \quad U_T = \frac{M_T}{Z_{11}} = \frac{M_T}{Z_T(\Lambda)}. \quad (\text{A.8})$$

the term U_L and U_T correspond to the physical longitudinal and Goldstone mass mode, respectively.

For later reference, in a flat background ($\bar{R} = 0$) and evaluated at the running minimum $U'(\bar{\rho}) = 0$, the transverse mass U_T vanishes (Goldstone modes), while the longitudinal one U_L reduces to the mass term used in Eq. (III.4) after conversion to dimensionless variables. In what follows we set $\bar{R} = 0$, since Z_L and Z_T are extracted from the scalar kinetic terms and we focus on the flat-background projection.

The functional trace is evaluated using the early-time heat-kernel expansion for a Laplace-type operator $\Delta = -\square + \mathbf{U}$,

$$\text{Tr}[W(\Delta)] = \frac{1}{(4\pi)^{d/2}} \int d^d x \sqrt{g} \sum_{n=0}^{\infty} b_{2n}(\Delta) Q_{d/2-n}[W], \quad (\text{A.9})$$

with (see e.g. [71–75])

$$\begin{aligned} b_0(\Delta) &= \text{tr } \mathbf{1}, & b_2(\Delta) &= \frac{1}{6} R \text{tr } \mathbf{1} - \text{tr } \mathbf{U}, \\ b_4(\Delta) &= -\frac{1}{6} \square \text{tr } \mathbf{U} + O(R^2), & b_6(\Delta) &= \text{tr} \left[\frac{1}{12} (\partial_\mu \mathbf{U})(\partial^\mu \mathbf{U}) + \frac{1}{6} \mathbf{U} \square \mathbf{U} \right] + O(R^3). \end{aligned} \quad (\text{A.10})$$

Here tr denotes the internal $O(N)$ trace only. The Q -functionals are Mellin transforms,

$$Q_p[W] = \frac{1}{\Gamma(p)} \int_0^\infty dz z^{p-1} W(z), \quad p > 0. \quad (\text{A.11})$$

where in our case, from eq.(A.1), we read $W(z) = e^{-s(Az+B)}$.

Since we work on a background without boundary (and ultimately set $\bar{R} = 0$), total derivatives can be dropped. In particular, the b_4 contribution is a total derivative, and in b_6 we may use $\square(\mathbf{U}^2) = 2(\mathbf{U} \square \mathbf{U} + (\partial \mathbf{U})^2)$ to trade the $\mathbf{U} \square \mathbf{U}$ term for $(\partial \mathbf{U})^2$ up to total derivatives. Thus, for the kinetic projection it is sufficient to keep the $(\partial \mathbf{U})^2$ structure.

C Derivative structure and separation into longitudinal/transverse sectors

We compute

$$\text{tr}[(\partial_\mu \mathbf{U})(\partial^\mu \mathbf{U})] = \sum_{a,b=1}^N \partial_\mu U_{ab} \partial^\mu U_{ba}. \quad (\text{A.12})$$

Using $\mathbf{U} = U_L P^L + U_T P^T$ and that $U_{L,T}$ are functions of ρ , one finds

$$\begin{aligned} \text{tr}[(\partial_\mu \mathbf{U})(\partial^\mu \mathbf{U})] &= (\partial_\mu \rho)(\partial^\mu \rho) \left[(U'_T)^2 \sum_{a,b} P_{ab}^T P_{ab}^T + (U'_L)^2 \sum_{a,b} P_{ab}^L P_{ab}^L \right] \\ &\quad + (U_L - U_T)^2 \sum_{a,b} (\partial_\mu P_{ab}^L)(\partial^\mu P_{ab}^L) \\ &\quad + 2(U_L - U_T)(\partial_\mu \rho) \sum_{a,b} [P_{ab}^L (\partial^\mu P_{ab}^L) U'_L + P_{ab}^T (\partial^\mu P_{ab}^L) U'_T]. \end{aligned} \quad (\text{A.13})$$

The required projector identities are

$$\sum_{a,b} P_{ab}^L P_{ab}^L = 1, \quad \sum_{a,b} P_{ab}^T P_{ab}^T = N - 1, \quad \sum_{a,b} P_{ab}^L (\partial^\mu P_{ab}^L) = 0, \quad \sum_{a,b} P_{ab}^T (\partial^\mu P_{ab}^L) = 0, \quad (\text{A.14})$$

and

$$\sum_{a,b}(\partial^\mu P_{ab}^L)(\partial_\mu P_{ab}^L) = -\frac{(\partial_\mu\rho)(\partial^\mu\rho)}{2\rho^2} + \frac{1}{\rho} \sum_{a=1}^N (\partial_\mu\phi_a)(\partial^\mu\phi_a). \quad (\text{A.15})$$

Therefore,

$$\begin{aligned} \text{tr}[(\partial_\mu \mathbf{U})(\partial^\mu \mathbf{U})] &= (\partial_\mu\rho)(\partial^\mu\rho) [(U'_T)^2(N-1) + (U'_L)^2] + \\ &\quad + (U_L - U_T)^2 \left[-\frac{(\partial_\mu\rho)(\partial^\mu\rho)}{2\rho^2} + \frac{1}{\rho} \sum_{a=1}^N (\partial_\mu\phi_a)(\partial^\mu\phi_a) \right]. \end{aligned} \quad (\text{A.16})$$

We now evaluate on an $O(N)$ -breaking background pointing in the N -direction, so that only the longitudinal background component is nonzero. In this case $(\partial_\mu\rho)(\partial^\mu\rho)$ projects onto the longitudinal fluctuation sector, while the transverse sector is isolated by the term proportional to $\sum_{a=1}^{N-1} (\partial_\mu\phi_a)(\partial^\mu\phi_a)$. Explicitly, after evaluating on the background,

$$b_6(\Delta) = \frac{1}{12} \text{tr}[(\partial_\mu \mathbf{U})(\partial^\mu \mathbf{U})] = b_{6,L} (\partial_\mu\phi_N)(\partial^\mu\phi_N) + b_{6,T} \sum_{a=1}^{N-1} (\partial_\mu\phi_a)(\partial^\mu\phi_a), \quad (\text{A.17})$$

with

$$b_{6,L} = \frac{1}{12} 2\bar{\rho} [(U'_T)^2(N-1) + (U'_L)^2], \quad b_{6,T} = \frac{1}{12} (U_L - U_T)^2 \frac{1}{\bar{\rho}}. \quad (\text{A.18})$$

D Proper-time integrals and flows of Z_L and Z_T

Keeping only the b_6 term in Eq. (A.9) and inserting Eq. (A.17) into the flow, we obtain

$$\begin{aligned} \Lambda \partial_\Lambda S_\Lambda &= \frac{1}{2} \int_0^\infty \frac{ds}{s} r(s, \Lambda^2 \mathbf{Z}) \frac{1}{(4\pi)^{d/2}} \int d^d x \sqrt{g} b_6(\Delta) Q_{d/2-3}[W] \\ &= \frac{1}{(4\pi)^{d/2}} \int d^d x \sqrt{g} \left\{ \left[\frac{1}{2} \int_0^\infty \frac{ds}{s} r(s, \Lambda^2 Z_T) b_{6,T} Q_{d/2-3}(W_T) \right] \sum_{a=1}^{N-1} (\partial_\mu\phi_a)(\partial^\mu\phi_a) \right. \\ &\quad \left. + \left[\frac{1}{2} \int_0^\infty \frac{ds}{s} r(s, \Lambda^2 Z_L) b_{6,L} Q_{d/2-3}(W_L) \right] (\partial_\mu\phi_N)(\partial^\mu\phi_N) \right\}, \end{aligned} \quad (\text{A.19})$$

where

$$W_L(z) = \exp[-s(Z_{NN}z + M_L)], \quad W_T(z) = \exp[-s(Z_T z + M_T)]. \quad (\text{A.20})$$

Matching to the left-hand side of Eq. (A.1) yields

$$\begin{aligned}\Lambda \partial_\Lambda Z_L &= -\frac{1}{(4\pi)^{d/2}} \int_0^\infty \frac{ds}{s} r(s, \Lambda^2 Z_L) \frac{1}{12} 2\bar{\rho} [(U'_T)^2(N-1) + (U'_L)^2] Q_{d/2-3}(W_L), \\ \Lambda \partial_\Lambda Z_T &= -\frac{1}{(4\pi)^{d/2}} \int_0^\infty \frac{ds}{s} r(s, \Lambda^2 Z_T) \frac{1}{12} (U_L - U_T)^2 \frac{1}{\bar{\rho}} Q_{d/2-3}(W_T).\end{aligned}\quad (\text{A.21})$$

Using the cutoff kernel in Eq. (I.2) (type-C: $\epsilon = 0$) one may perform the z -integral in Q_p and then the s -integral. A convenient identity is

$$\frac{1}{2} \int_0^\infty \frac{ds}{s} r(s, \Lambda^2 A) Q_p(W = e^{-s(Az+B)}) = (\gamma \Lambda^2)^p \left(1 + \frac{B}{A\gamma \Lambda^2}\right)^{p-m} \frac{\Gamma(m-p)}{(4\pi)^{d/2} \Gamma(m)}, \quad p = \frac{d}{2} - j, \quad (\text{A.22})$$

which is to be used with $A = Z_{NN}$, $B = M_L$ (longitudinal) or $A = Z_T$, $B = M_T$ (transverse), and $j = 3$ for the present projection.

Inserting Eq. (A.22) and rewriting $\partial_t \equiv \Lambda \partial_\Lambda$ finally yields

$$\begin{aligned}\partial_t Z_L &= -\frac{(\gamma \Lambda^2)^{\frac{d-6}{2}}}{3(4\pi)^{\frac{d}{2}}} \frac{\Gamma(m - \frac{d}{2} + 3)}{\Gamma(m)} \left(1 + \frac{\bar{U}' + 2\bar{\rho}\bar{U}''}{\gamma \Lambda^2 Z_L \left(1 + \frac{4(d-1)\bar{\rho}(\bar{F}')^2}{(d-2)Z_L F}\right)}\right)^{\frac{d}{2}-(m+3)} \left[\frac{\bar{\rho}(\bar{U}'')^2}{Z_T^2} (N-1) + \right. \\ &\quad \left. + \frac{4\bar{\rho}^2\bar{U}''' - 3\bar{U}'}{4\bar{\rho}Z_L^2 \left(1 + \frac{4(d-1)\bar{\rho}(\bar{F}')^2}{(d-2)Z_L F}\right)^2} \left(1 + \frac{\bar{U}' + 2\bar{\rho}\bar{U}''}{4\bar{\rho}^2\bar{U}''' - 3\bar{U}'} \left(1 + \frac{2 \left(1 + \frac{4(d-1)\bar{\rho}^2\bar{F}'}{(d-2)Z_L F} \left(\frac{(\bar{F}')^2}{F} - 2\bar{F}''\right)\right)}{1 + \frac{4(d-1)\bar{\rho}(\bar{F}')^2}{(d-2)Z_L F}}\right)^2\right)\right],\end{aligned}\quad (\text{A.23})$$

and

$$\partial_t Z_T = -\frac{(\gamma \Lambda^2)^{\frac{d-6}{2}}}{6(4\pi)^{d/2} \bar{\rho}} \frac{\Gamma(m - \frac{d}{2} + 3)}{\Gamma(m)} \left(1 + \frac{\bar{U}'}{\gamma \Lambda^2 Z_T}\right)^{\frac{d}{2}-(m+3)} \left(\frac{\bar{U}'}{Z_T} - \frac{\bar{U}' + 2\bar{\rho}\bar{U}''}{Z_L \left(1 + \frac{4(d-1)\bar{\rho}(\bar{F}')^2}{(d-2)Z_L F}\right)}\right)^2. \quad (\text{A.24})$$

A bar indicates evaluation on the background. Using the definitions in Eq. (II.5) and the dimensionless variables $x = Z_L \Lambda^{2-d} \rho$, $u_\Lambda(x) = \Lambda^{-d} U_\Lambda(\rho)$, and $f_\Lambda(x) = \Lambda^{2-d} F_\Lambda(\rho)$, one obtains the anomalous dimensions reported in Eq. (II.12).

E Consistency check: the $N = 1$ limit

It is instructive to verify how the $N = 1$ case is recovered. In Eq. (A.16), the transverse contribution is proportional to

$$-\frac{(\partial_\mu \rho)(\partial^\mu \rho)}{2\rho^2} + \frac{1}{\rho} \sum_{a=1}^N (\partial_\mu \phi_a)(\partial^\mu \phi_a).$$

For $N = 1$, $\rho = \phi^2/2$ and $(\partial_\mu \rho)(\partial^\mu \rho) = \phi^2(\partial_\mu \phi)(\partial^\mu \phi)$, hence

$$-\frac{(\partial_\mu \rho)(\partial^\mu \rho)}{2\rho^2} + \frac{1}{\rho} (\partial_\mu \phi)(\partial^\mu \phi) = -\frac{\phi^2(\partial_\mu \phi)(\partial^\mu \phi)}{2(\phi^4/4)} + \frac{(\partial_\mu \phi)(\partial^\mu \phi)}{\phi^2/2} = 0. \quad (\text{A.25})$$

Therefore only the longitudinal contribution remains, as expected.

B THE BETA FUNCTIONS

In this appendix we derive the beta functions for the ansats

$$\begin{aligned} u_t(x) &= u_0(t) + \lambda(t) (x - x_0(t))^2 + O((x - x_0(t))^3) \\ f_t(x) &= \frac{1}{g(t)} + f_1(t) (x - x_0(t)) + O((x - x_0(t))^2). \end{aligned} \quad (\text{B.1})$$

The beta functions can be found replacing the ansats in eqs.(II.10) and expanding in series around $x = x_0$.

In $d = 4$ the flow equation for u_0 is given by

$$\dot{u}_0 = -4u_0 + \frac{\gamma^2}{16\pi^2} \frac{\Gamma(m-2)}{\Gamma(m)} \left(N + 1 + \left(1 + \frac{4\lambda x_0}{\gamma(1+6f_1^2gx_0)} \right)^{2-m} \right) \quad (\text{B.2})$$

The flow equation for x_0 is given by

$$\dot{x}_0 = -(2 + \eta_L) x_0 + \frac{\gamma}{16\pi^2(m-1)} \left(\frac{N-1}{w} + \frac{3(1+2f_1^2gx_0+4f_1^3g^2x_0^2)}{(1+6f_1^2gx_0)^2 \left(1 + \frac{4\lambda x_0}{\gamma(1+6f_1^2gx_0)} \right)^{m-1}} \right) \quad (\text{B.3})$$

The flow equation for λ is given by

$$\begin{aligned} \dot{\lambda} = \lambda & \left(2\eta_L + \frac{9\gamma f_1^2 g (1 - f_1 g x_0) (1 + 2f_1 g x_0 (f_1 - \frac{1}{3}))}{4\pi^2 (m-1) (1 + 6f_1^2 g x_0)^3 \left(1 + \frac{4\lambda x_0}{\gamma(1+6f_1^2 g x_0)} \right)^m} \right) + \\ & + \frac{\lambda^2}{8\pi^2 (m-1)} \left(\frac{(m-1)(N-1)}{w^2} + \frac{3C(t)}{(1 + 6f_1^2 g x_0)^4 \left(1 + \frac{4\lambda x_0}{\gamma(1+6f_1^2 g x_0)} \right)^m} \right) \end{aligned} \quad (\text{B.4})$$

where

$$\begin{aligned} C(t) = 3(m-1) + 12g(1+m)f_1^2 x_0 + 4f_1^3 g^2 x_0^2 (6m-16+3(3+m)f_1) + \\ + 16f_1^4 g^3 x_0^3 (1+3(m-2)f_1) + 48f_1^6 g^4 x_0^4 (m-1) \end{aligned} \quad (\text{B.5})$$

The flow equation for g is given by

$$\dot{g} = 2g + \frac{\gamma g^2}{6\pi^2 (m-1)} \left(\frac{N-1}{16} - 1 + \frac{1 - 12f_1 + 12f_1^2 g x_0 (2 + 3g f_1^2 x_0)}{16 (1 + 6f_1^2 g x_0)^2 \left(1 + \frac{4\lambda x_0}{\gamma(1+6f_1^2 g x_0)} \right)^{m-1}} \right) \quad (\text{B.6})$$

The flow equation of f_1 is given by

$$\begin{aligned} \dot{f}_1 = f_1 \eta_L + \frac{1}{8\pi^2 (m-1)} \left\{ \frac{\lambda}{w} \left(\frac{1}{6} + \frac{f_1}{w} \right) (m-1)(N-1) + \right. \\ + \frac{1}{(1 + 6f_1^2 g x_0)^2 \left(1 + \frac{4\lambda x_0}{\gamma(6f_1^2 g x_0 + 1)} \right)^m} \left[3\gamma f_1^2 g \left(f_1 - \frac{1}{3} \right) (1 - f_1 g x_0) \left(1 + \frac{4\lambda x_0}{\gamma(6f_1^2 g x_0 + 1)} \right) + \right. \\ \left. \left. + \frac{\lambda (m-1) (1 + 2f_1^2 g x_0 (1 + 2f_1 g x_0)) (1 + 6f_1 (1 + 3f_1 g x_0))}{2 (1 + 6f_1^2 g x_0)} \right] \right\} \end{aligned} \quad (\text{B.7})$$

All beta functions do not depend on u_0 , consequently the equations are decoupled with respect to the flow of u_0 . In the flow equations, the quantity $\frac{4\lambda x_0}{1+6f_1^2 g x_0}$ is the dimensionless longitudinal scalar mass. The flow equations do not depend on η_T and the presence of Z_T appears only by w . The presence of η_L breaks the classical marginality of λ , f_1 and shifts the classical scaling of x_0 . The flow of g can be written in the standard form $\dot{g} = (d-2+\eta_g)g$. The gravitational anomalous dimension η_g does not depend on w and η_L whereas λ appears only by the presence

of the longitudinal scalar mass.

In the full flow equations eqs.(II.10) the potential is coupled to gravity only by $f'(x)$. In term of ansats eq.(B.1), this translates in the flow of λ coupled to the newtonian constant only by f_1 . This is a feature of the physical gauge. The origin of this can be found writing the pysical gauge in terms of background field gauge method. With the standard notation of [76], the physical gauge is the limit $\beta \rightarrow \infty$ and $\alpha \rightarrow 0$. In the flow equations for general β and α the newtonian constant always appears in the form $\sim g/\beta$ [76]. Accordingly, in the limit $\beta \rightarrow \infty$ the standard terms disappear and g is coupled to the potential only if the newtonian constant has a field dependence.

The flow equation for $w(t)$ is given by

$$\dot{w}(t) = w(t)(\eta_L - \eta_T) \quad (\text{B.8})$$

The equation for η_L and η_T can be derived simply replacing the ansatz in eq.(II.12) and putting $x = x_0$. The results are

$$\begin{aligned} \eta_L &= \frac{\lambda^2 x_0 m}{12\pi^2 \gamma \left(1 + \frac{4\lambda x_0}{\gamma(1+6f_1^2gx_0)}\right)^{m+1}} \left(\frac{N-1}{w^2} + 9 \left(\frac{1+2f_1^2gx_0(1+2f_1gx_0)}{(1+6f_1^2gx_0)^2} \right)^2 \right) \\ \eta_T &= \frac{\lambda^2 mx_0}{6\gamma w \pi^2 (1+6f_1^2gx_0)^2} \end{aligned} \quad (\text{B.9})$$

In this way the flow equation of w is given by

$$\dot{w} = \frac{\lambda^2 mx_0}{6\gamma \pi^2} \left[\frac{\frac{N-1}{w} + 9w \left(\frac{1+2f_1^2gx_0(1+2f_1gx_0)}{(1+6f_1^2gx_0)^2} \right)^2}{2 \left(1 + \frac{4\lambda x_0}{\gamma(6f_1^2gx_0+1)} \right)^{m+1}} - \frac{1}{(1+6f_1^2gx_0)^2} \right] \quad (\text{B.10})$$

from eq.(B.9) we see that at the fixed point $\lambda_* = 0$ the two anomalous dimensions vanish, so w_* is a free parameter.

[1] D. Buttazzo, G. Degrassi, P. P. Giardino, G. F. Giudice, F. Sala, A. Salvio, and A. Strumia, Investigating the near-criticality of the Higgs boson, *JHEP* **12**, 089, arXiv:1307.3536 [hep-ph].

- [2] A. A. Starobinsky, A New Type of Isotropic Cosmological Models Without Singularity, *Phys. Lett. B* **91**, 99 (1980).
- [3] A. H. Guth, The Inflationary Universe: A Possible Solution to the Horizon and Flatness Problems, *Phys. Rev. D* **23**, 347 (1981).
- [4] V. F. Mukhanov and G. V. Chibisov, Quantum Fluctuations and a Nonsingular Universe, *JETP Lett.* **33**, 532 (1981).
- [5] A. D. Linde, Chaotic Inflation, *Phys. Lett. B* **129**, 177 (1983).
- [6] Q. Shafi and C. Wetterich, Cosmology from Higher Dimensional Gravity, *Phys. Lett. B* **129**, 387 (1983).
- [7] F. L. Bezrukov and M. Shaposhnikov, The Standard Model Higgs boson as the inflaton, *Phys. Lett. B* **659**, 703 (2008), arXiv:0710.3755 [hep-th].
- [8] M. Herranen, T. Markkanen, S. Nurmi, and A. Rajantie, Spacetime curvature and the Higgs stability during inflation, *Phys. Rev. Lett.* **113**, 211102 (2014), arXiv:1407.3141 [hep-ph].
- [9] M. Li, X.-D. Li, S. Wang, and Y. Wang, Dark Energy: A Brief Review, *Front. Phys. (Beijing)* **8**, 828 (2013), arXiv:1209.0922 [astro-ph.CO].
- [10] E. Oks, Brief review of recent advances in understanding dark matter and dark energy, *New Astron. Rev.* **93**, 101632 (2021), arXiv:2111.00363 [astro-ph.CO].
- [11] M. Cirelli, A. Strumia, and J. Zupan, Dark Matter (2024), arXiv:2406.01705 [hep-ph].
- [12] A. Arbey and F. Mahmoudi, Dark matter and the early Universe: a review, *Prog. Part. Nucl. Phys.* **119**, 103865 (2021), arXiv:2104.11488 [hep-ph].
- [13] N. Christiansen, D. F. Litim, J. M. Pawłowski, and M. Reichert, Asymptotic safety of gravity with matter, *Phys. Rev. D* **97**, 106012 (2018), arXiv:1710.04669 [hep-th].
- [14] B. Bürger, J. M. Pawłowski, M. Reichert, and B.-J. Schaefer, Curvature dependence of quantum gravity with scalars (2019), arXiv:1912.01624 [hep-th].
- [15] A. Eichhorn, S. Lippoldt, and M. Schiffer, Zooming in on fermions and quantum gravity, *Phys. Rev. D* **99**, 086002 (2019), arXiv:1812.08782 [hep-th].
- [16] N. Alkofer and F. Saueressig, Asymptotically safe $f(R)$ -gravity coupled to matter I: the polynomial case, *Annals Phys.* **396**, 173 (2018), arXiv:1802.00498 [hep-th].
- [17] J. Biemans, A. Platania, and F. Saueressig, Renormalization group fixed points of foliated gravity-matter systems, *JHEP* **05**, 093, arXiv:1702.06539 [hep-th].
- [18] K.-y. Oda and M. Yamada, Non-minimal coupling in Higgs–Yukawa model with asymptotically safe gravity, *Class. Quant. Grav.* **33**, 125011 (2016), arXiv:1510.03734 [hep-th].
- [19] J. Meibohm, J. M. Pawłowski, and M. Reichert, Asymptotic safety of gravity-matter systems, *Phys. Rev. D* **93**, 084035 (2016), arXiv:1510.07018 [hep-th].
- [20] P. Donà, A. Eichhorn, and R. Percacci, Matter matters in asymptotically safe quantum gravity, *Phys. Rev. D* **89**, 084035 (2014), arXiv:1311.2898 [hep-th].

- [21] C. Wetterich, The Quantum Gravity Connection between Inflation and Quintessence, *Galaxies* **10**, 50 (2022), arXiv:2201.12213 [astro-ph.CO].
- [22] J. M. Pawłowski, M. Reichert, C. Wetterich, and M. Yamada, Higgs scalar potential in asymptotically safe quantum gravity, *Phys. Rev. D* **99**, 086010 (2019), arXiv:1811.11706 [hep-th].
- [23] C. Wetterich, Effective scalar potential in asymptotically safe quantum gravity, *Universe* **7**, 45 (2021), arXiv:1911.06100 [hep-th].
- [24] C. Wetterich and M. Yamada, Variable Planck mass from the gauge invariant flow equation, *Phys. Rev. D* **100**, 066017 (2019), arXiv:1906.01721 [hep-th].
- [25] I. L. Shapiro, P. Morais Teixeira, and A. Wipf, On the functional renormalization group for the scalar field on curved background with non-minimal interaction, *Eur. Phys. J. C* **75**, 262 (2015), arXiv:1503.00874 [hep-th].
- [26] B. S. Merzlikin, I. L. Shapiro, A. Wipf, and O. Zanusso, Renormalization group flows and fixed points for a scalar field in curved space with nonminimal $F(\phi)R$ coupling, *Phys. Rev. D* **96**, 125007 (2017), arXiv:1711.02224 [hep-th].
- [27] M. Shaposhnikov and C. Wetterich, Asymptotic safety of gravity and the Higgs boson mass, *Phys. Lett. B* **683**, 196 (2010), arXiv:0912.0208 [hep-th].
- [28] T. R. Morris, The Exact renormalization group and approximate solutions, *Int. J. Mod. Phys. A* **9**, 2411 (1994), arXiv:hep-ph/9308265.
- [29] C. Wetterich, Exact evolution equation for the effective potential, *Physics Letters B* **301**, 90 (1993).
- [30] U. Ellwanger, FFlow equations for N point functions and bound states, *Z. Phys. C* **62**, 503 (1994), arXiv:hep-ph/9308260.
- [31] Á. Pastor-Gutiérrez, J. M. Pawłowski, and M. Reichert, The Asymptotically Safe Standard Model: From quantum gravity to dynamical chiral symmetry breaking, *SciPost Phys.* **15**, 105 (2023), arXiv:2207.09817 [hep-th].
- [32] A. Eichhorn and A. Held, Mass difference for charged quarks from asymptotically safe quantum gravity, *Phys. Rev. Lett.* **121**, 151302 (2018), arXiv:1803.04027 [hep-th].
- [33] J. P. Garcés, F. Goertz, M. Lindner, and Á. Pastor-Gutiérrez, The quantum criticality of the Standard Model and the hierarchy problem, *JHEP* **10**, 134, arXiv:2506.15919 [hep-ph].
- [34] C. Wetterich and M. Yamada, Gauge hierarchy problem in asymptotically safe gravity—the resurgence mechanism, *Phys. Lett. B* **770**, 268 (2017), arXiv:1612.03069 [hep-th].
- [35] Y. Hamada and M. Yamada, Asymptotic safety of higher derivative quantum gravity non-minimally coupled with a matter system, *JHEP* **08**, 070, arXiv:1703.09033 [hep-th].
- [36] A. Eichhorn and A. Held, Top mass from asymptotic safety, *Phys. Lett. B* **777**, 217 (2018), arXiv:1707.01107 [hep-th].
- [37] M. Hashimoto, S. Iso, and Y. Orikasa, Radiative symmetry breaking at the Fermi scale and flat potential at the Planck scale, *Phys. Rev. D* **89**, 016019 (2014), arXiv:1310.4304 [hep-ph].

- [38] M. Hashimoto, S. Iso, and Y. Orikasa, Radiative symmetry breaking from flat potential in various $U(1)'$ models, *Phys. Rev. D* **89**, 056010 (2014), arXiv:1401.5944 [hep-ph].
- [39] A. Eichhorn, Status update: Asymptotically safe gravity-matter systems, *Nuovo Cim. C* **45**, 29 (2022), arXiv:2201.11543 [gr-qc].
- [40] A. Eichhorn and M. Schiffer, Asymptotic safety of gravity with matter (2022), arXiv:2212.07456 [hep-th].
- [41] A. Eichhorn and M. Schiffer, $d = 4$ as the critical dimensionality of asymptotically safe interactions, *Phys. Lett. B* **793**, 383 (2019), arXiv:1902.06479 [hep-th].
- [42] A. Eichhorn, A. Held, and C. Wetterich, Quantum-gravity predictions for the fine-structure constant, *Phys. Lett. B* **782**, 198 (2018), arXiv:1711.02949 [hep-th].
- [43] A. Eichhorn and F. Versteegen, Upper bound on the Abelian gauge coupling from asymptotic safety, *JHEP* **01**, 030, arXiv:1709.07252 [hep-th].
- [44] A. Eichhorn, An asymptotically safe guide to quantum gravity and matter, *Front. Astron. Space Sci.* **5**, 47 (2019), arXiv:1810.07615 [hep-th].
- [45] A. Eichhorn, Y. Hamada, J. Lumma, and M. Yamada, Quantum gravity fluctuations flatten the Planck-scale Higgs potential, *Phys. Rev. D* **97**, 086004 (2018), arXiv:1712.00319 [hep-th].
- [46] M. Reichert and J. Smirnov, Dark Matter meets Quantum Gravity, *Phys. Rev. D* **101**, 063015 (2020), arXiv:1911.00012 [hep-ph].
- [47] Y. Hamada, K. Tsumura, and M. Yamada, Scalegenesis and fermionic dark matters in the flatland scenario, *Eur. Phys. J. C* **80**, 368 (2020), arXiv:2002.03666 [hep-ph].
- [48] A. Eichhorn and M. Pauly, Safety in darkness: Higgs portal to simple Yukawa systems, *Phys. Lett. B* **819**, 136455 (2021), arXiv:2005.03661 [hep-ph].
- [49] V. Fock, Proper time in classical and quantum mechanics, *Phys. Z. Sowjetunion* **12**, 404 (1937).
- [50] J. Schwinger, On gauge invariance and vacuum polarization, *Phys. Rev.* **82**, 664 (1951).
- [51] A. Bonanno and D. Zappala, Towards an accurate determination of the critical exponents with the renormalization group flow equations, *Phys. Lett. B* **504**, 181 (2001), arXiv:hep-th/0010095.
- [52] M. Mazza and D. Zappala, Proper time regulator and renormalization group flow, *Phys. Rev. D* **64**, 105013 (2001), arXiv:hep-th/0106230.
- [53] S.-B. Liao, On connection between momentum cutoff and the proper time regularizations, *Phys. Rev. D* **53**, 2020 (1996), arXiv:hep-th/9501124.
- [54] S.-B. Liao, Operator cutoff regularization and renormalization group in Yang-Mills theory, *Phys. Rev. D* **56**, 5008 (1997), arXiv:hep-th/9511046.
- [55] B.-J. Schaefer and H.-J. Pirner, Renormalization group flow and equation of state of quarks and mesons, *Nucl. Phys. A* **660**, 439 (1999), arXiv:nucl-th/9903003.
- [56] B. J. Schaefer, O. Bohr, and J. Wambach, Finite temperature gluon condensate with renormalization group flow equations, *Phys. Rev. D* **65**, 105008 (2002), arXiv:hep-th/0112087.

- [57] O. Bohr, B. J. Schaefer, and J. Wambach, Renormalization group flow equations and the phase transition in $O(N)$ models, *Int. J. Mod. Phys. A* **16**, 3823 (2001), [arXiv:hep-ph/0007098](https://arxiv.org/abs/hep-ph/0007098).
- [58] D. Zappala', Improving the renormalization group approach to the quantum mechanical double well potential, *Phys. Lett. A* **290**, 35 (2001), [arXiv:quant-ph/0108019](https://arxiv.org/abs/quant-ph/0108019).
- [59] D. F. Litim and D. Zappala, Ising exponents from the functional renormalisation group, *Phys. Rev. D* **83**, 085009 (2011), [arXiv:1009.1948 \[hep-th\]](https://arxiv.org/abs/1009.1948).
- [60] A. Bonanno, A. Codello, and D. Zappala', Structural aspects of FRG in quantum tunneling computations, *Annals Phys.* **445**, 169090 (2022), [arXiv:2206.06917 \[hep-th\]](https://arxiv.org/abs/2206.06917).
- [61] E. M. Glaviano and A. Bonanno, Proper-time flow equation and non-local truncations in quantum gravity, in *17th Marcel Grossmann Meeting: On Recent Developments in Theoretical and Experimental General Relativity, Gravitation, and Relativistic Field Theories* (2024) [arXiv:2410.23696 \[gr-qc\]](https://arxiv.org/abs/2410.23696).
- [62] G. Giacometti, D. Rizzo, and D. Zappala, On the universal content of the proper time flow in scalar and Yang-Mills theories (2025), [arXiv:2510.04896 \[hep-th\]](https://arxiv.org/abs/2510.04896).
- [63] A. Bonanno, G. Oglialoro, and D. Zappalà, Gauge and parametrization dependence of quantum Einstein gravity within the proper time flow, *Phys. Rev. D* **112**, 026002 (2025), [arXiv:2504.07877 \[hep-th\]](https://arxiv.org/abs/2504.07877).
- [64] A. Bonanno, S. Lippoldt, R. Percacci, and G. P. Vacca, On Exact Proper Time Wilsonian RG Flows, *Eur. Phys. J. C* **80**, 249 (2020), [arXiv:1912.08135 \[hep-th\]](https://arxiv.org/abs/1912.08135).
- [65] A. Bonanno and M. Reuter, Proper time flow equation for gravity, *JHEP* **02**, 035, [arXiv:hep-th/0410191](https://arxiv.org/abs/hep-th/0410191).
- [66] A. Bonanno, E. Glaviano, and G. P. Vacca, Proper-time functional renormalization in $O(N)$ scalar models coupled to gravity (2025), [arXiv:2508.00807 \[hep-th\]](https://arxiv.org/abs/2508.00807).
- [67] R. Percacci and G. P. Vacca, Search of scaling solutions in scalar-tensor gravity, *Eur. Phys. J. C* **75**, 188 (2015), [arXiv:1501.00888 \[hep-th\]](https://arxiv.org/abs/1501.00888).
- [68] N. Ohta, R. Percacci, and G. P. Vacca, Renormalization Group Equation and scaling solutions for $f(R)$ gravity in exponential parametrization, *Eur. Phys. J. C* **76**, 46 (2016), [arXiv:1511.09393 \[hep-th\]](https://arxiv.org/abs/1511.09393).
- [69] P. Labus, R. Percacci, and G. P. Vacca, Asymptotic safety in $O(N)$ scalar models coupled to gravity, *Phys. Lett. B* **753**, 274 (2016), [arXiv:1505.05393 \[hep-th\]](https://arxiv.org/abs/1505.05393).
- [70] C. D. Dijkstra, Naturalness as a reasonable scientific principle in fundamental physics (2019), [arXiv:1906.03036 \[physics.hist-ph\]](https://arxiv.org/abs/1906.03036).
- [71] A. O. Barvinsky and G. A. Vilkovisky, Covariant perturbation theory. 2: Second order in the curvature. General algorithms, *Nucl. Phys. B* **333**, 471 (1990).
- [72] A. O. Barvinsky and G. A. Vilkovisky, Beyond the schwinger-dewitt technique: Converting loops into trees and in-in currents, *Nuclear Physics* **282**, 163 (1987).

- [73] A. O. Barvinsky and G. A. Vilkovisky, Covariant perturbation theory. 3: Spectral representations of the third order form-factors, *Nucl. Phys. B* **333**, 512 (1990).
- [74] A. O. Barvinsky, Y. V. Gusev, V. V. Zhytnikov, and G. A. Vilkovisky, Covariant perturbation theory. 4. Third order in the curvature (1993), [arXiv:0911.1168 \[hep-th\]](https://arxiv.org/abs/0911.1168).
- [75] I. G. Avramidi, *Heat kernel and quantum gravity*, Vol. 64 (Springer, New York, 2000).
- [76] N. Ohta and M. Yamada, Higgs scalar potential coupled to gravity in the exponential parametrization in arbitrary gauge, *Phys. Rev. D* **105**, [10.1103/PhysRevD.105.026013](https://doi.org/10.1103/PhysRevD.105.026013) (2022), [arXiv:2110.08594 \[hep-th\]](https://arxiv.org/abs/2110.08594).